NASA TECHNICAL MEMORANDUM

NASA TM X-68222

NASA TM X-68222

PRELIMINARY APPRAISAL OF HYDROGEN AND METHANE FUEL IN A MACH 2.7 SUPERSONIC TRANSPORT

by John B. Whitlow, Jr., Richard J. Weber, and Kestutis C. Civinskas

Lewis Research Center and
U.S. Army Air Mobility R&D Laboratory
Cleveland, Ohio 44135

This information is being published in preliminary form in order to expedite its early release.

ABSTRACT

The higher heating value of hydrogen relative to JP fuel is estimated to reduce fuel weight by three fold and gross weight by 40 percent for comparably designed airplanes of equal payload and range. No advantage was found for turbine rotor-inlet temperatures higher than 2725° F, regardless of fuel type, for duct-burning turbofan engines constrained by FAR 36 noise limits. Engine design parameters were varied to determine the influence of lower noise goals on gross weight and direct operating cost. At current fuel prices, the DOC of a hydrogen airplane would be much higher than that of a JP airplane. A methane airplane could offer an 8.5-percent lower DOC than JP. But future shortages may escalate the prices of both JP and methane, whereas the price of hydrogen manufactured hydrolytically could be reduced from present levels. If in the future all three fuels are postulated to have equal costs per unit of energy, the DOC for hydrogen could be as much as 20 percent below that for JP on the reference 4000-nautical-mile mission. Longer ranges or lower noise requirements would improve the advantage of hydrogen. The additional complexities of developing and operating cryogenic systems would undoubtedly pare some of the apparent advantage.

E-7425

PRELIMINARY APPRAISAL OF HYDROGEN AND METHANE FUEL IN A MACH 2.7 SUPERSONIC TRANSPORT

by John B. Whitlow, Jr., Richard J. Weber, and Kestutis C. Civinskas

Lewis Research Center and
U.S. Army Air Mobility R&D Laboratory

SUMMARY

The higher heating value of hydrogen relative to conventional JP fuel is estimated to reduce fuel weight by three fold and gross weight by 40 percent for comparably designed airplanes carrying 250 passengers for a range of 4000 nautical miles. No further benefit was found by applying the cooling capacity of hydrogen to raise turbine rotor-inlet temperature beyond the 2725° F assumed for JP engines, provided that the engine jet noise is held constant. The direct operating cost of the hydrogen airplane is 1.68 cents per available seat-statute mile against 1.52 for JP, assuming fuel prices of 194 and 89 cents per million Btu, respectively. The gross weight of the methane airplane is only slightly lower than the JP, but its DOC is 1.39 cents if liquefied natural gas is available at 75 cents per million Btu. The fuel prices used here approximate recent delivered prices for the fossil fuels and an optimistically low future price for hydrogen. The quoted gross weights and DOC's are for a sideline noise limit approximately equal to those specified by FAR 36. Lower noise goals or other changes that make the mission more difficult tend to improve the relative attractiveness of hydrogen. However, this study does not consider the technological difficulties of developing and operating cryogenic aircraft, cost of ground fueling systems, safety, etc.

E-7425

INTRODUCTION

The use of liquid hydrogen fuel as a substitute for conventional kerosene or JP has been considered many times in the past (e.g., refs. 1 and 2). The interest at that time was principally due to the desire for improved performance of military airplanes. Further interest was for hypersonic applications, which have severe heating loads (e.g., refs. 3 and 4). More recently, renewed interest has arisen because of the potential for decreased pollution (ref. 5) or because of concern over depletion of fossil fuels (ref. 6).

This paper reports the results of a brief study of the performance and economics of a hydrogen-fueled commercial supersonic transport. For comparison, results are also given for JP-fueled airplanes and for methane-fueled airplanes, the latter fuel having been suggested in recent years as a promising alternative to JP (e.g., refs. 7 and 8).

Tables I(a) and (b) compare the fuel properties that are important to this type of study. The low boiling temperatures of the liquid gases pose obvious insulation problems. Their improved heating value and cooling capacity relative to JP offer hope of better specific fuel consumption and lighter engines. The increased volume required for fuel containment threatens weight and aerodynamic penalties. And the economics will obviously be highly sensitive to fuel price.

ANALYSIS

Mission

In order to compare the fuels on a consistent basis, they were all applied to a specific mission: namely, to transport 250 passengers for a range of 4000 nautical miles. Cruise Mach number is 2.7, cruise altitude is optimized, and no subsonic cruise legs are included. The climb and acceleration flight path is described in Mach number and altitude coordinates in figure 1. Reserves are provided to allow an additional 7 percent of the mission fuel, plus a 261-nautical-mile diversion at Mach 2.7 to an alternate airport, plus a 30-minute hold at Mach 0.5 and 15 000-feet altitude. Engine and airplane parameters were then selected to yield minimum takeoff gross weight while observing a specified sideline noise limit.

Airframe

An advanced arrow-wing (SCAT 15F-type) configuration was selected. This type of design has been extensively developed for JP fuel by the NASA-Langley Research Center. As shown in the upper half of the sketch of figure 2, the JP fuel is contained in wing tanks and in the lower portion of the fuselage. The low density of the cryogenic fuels requires that much larger volumes must be provided for their containment. Because of the difficulty of providing this additional volume in the shallow wings and because of the problems of insulating such tanks against aerodynamic heating, the required additional volume was provided within the fuselage, as shown for hydrogen fuel in the lower half of the sketch. The bottom-fuselage tanks were extended forward, and full-diameter tanks were placed in the rear. Also, the fuselage diameter was increased from 11.4 feet for JP (5 seats abreast) to 13.0 feet (6 abreast) for methane, and to 16.4 feet (7 abreast, double-aisle) for hydrogen. Fuselage length was then varied as required to match the fuel volume to the fuel load that yielded the desired range. Wing size varied with gross weight because optimum takeoff wing loading tends to be constant regardless of fuel.

Reference JP airplane. - The component weights of a reference, JP fueled airplane with a gross weight of 750 000 pounds and 250 seats are

given in table II. Takeoff wing loading for this airplane is 60 pounds per square foot. A previous study (ref. 9) indicated that this wing loading would maximize the range with JP-fueled dry turbojets meeting the FAR 36 sideline noise constraint of 108 EPNdB. Similar results are expected for the noise-constrained duct-burning turbofan engines used in this study. The component weights shown in table II are based on unpublished industry data for similar airplanes with no composite structure. Adjustments were made in arriving at the weights shown in table II to account for changes in wing loading, gross weight, and seating accommodations.

The wing weight represents the major adjustment from industry data, since the wing loading used in this study is somewhat lower than that usually obtained in prior studies where FAR 36 sideline noise was not a constraint. An equation was developed, based on empirical data (ref. 10), which corrects an industry SCAT 15F-type wing-weight data point to a wing loading of 60 pounds per square foot and a gross weight of 750 000 pounds, as follows:

$$W_{wing} = (W_{wing})_{ref}\left[\frac{(W_g/S)_{ref}}{60} \times \left(\frac{750\ 000}{(W_g)_{ref}}\right)^2\right]^{0.64} \qquad (1)$$

The landing gear weight was adjusted by assuming that it would remain a constant fraction of the takeoff gross weight. Body weight was adjusted by allowing it to vary in proportion to length, since the diameter and nominal five-abreast seating configuration were not altered as the number of seats was increased to 250 from a reference of 200. The tail weight was scaled directly with wing area from the reference point. The weight of fixed equipment was also changed a small amount to account for a change in design payload.

The propulsion system weight was not based on the afterburning turbojets used in most of the previous industry studies, but rather on the weight estimated for installed unsuppressed duct-burning turbofan engines. (The turbofan engine was used because of its lower jet noise characteristics.) A description of the weight estimation procedure used for the propulsion system appears later in a section on engines. The propulsion system weight listed in table II includes four engines with inlets, nacelles, nozzles, accessories, and fixed installation weight. The particular engines tabulated here each have a sea-level-static corrected airflow of 1235 pounds per second, a bypass ratio of 2.0, a fan pressure ratio of 3.0, and an overall fan-plus-compressor pressure ratio of 10. With the duct burner unlit at takeoff, they produce at design turbine temperature a sideline noise approximating the FAR 36 limit.

Hydrogen-fuel tankage dimensions and weights. - With cryogenic fuels, it was decided at the outset that storage of significant amounts of fuel in the wings would very likely not be desirable because of the additional

heating loads and the poor volumetric efficiency after allowing for insulation volume and tank shape requirements. Relatively large insulation and tank weight penalties would likely be incurred with fuel in the wing. It did not seem desirable to increase the wing area and depth to accommodate larger, more optimally-shaped tanks because the wing of a conventionally-fueled airplane already represents such a significant part of the structural weight (see table II). Larger wings would thus represent a larger structural weight.

Most of the fuel was stored in the fuselage. A tank volume of only 1170 cubic feet was assigned to the wing of the cryogenically-fueled airplanes. This volume was allocated near the wing root chord where thickness is greatest. Allowance was made for approximately 6 inches of space around the outside of each tank to accommodate insulation. Allowance was also made for landing gear struts, actuators, etc., and trailing-edge flaps in locating these tanks. (A wing tank capacity of 1760 cubic feet was allowed for the conventionally-fueled airplanes.)

As a starting point for the calculations, it was assumed that about 100 000 pounds of liquid hydrogen fuel would be needed for a 250-passenger airplane on a 4000-nautical-mile mission. This would necessitate a fuel storage volume of about 23 000 cubic feet. Only about one-third of this, at most, could be accommodated under the passengers in a fuselage with the five-abreast seating arrangement used with JP fuel. A fuselage extension of about 180 feet would be required to accommodate the rest of the fuel in full-diameter (10.4-ft) tanks. Such an extension would represent an increase of more than 50 percent in the already-slim fuselage of the JP configuration. The alternative is to increase the body diameters.

A seven-abreast seating arrangement with a double aisle was ultimately chosen for hydrogen fuel because of the more acceptable fuselage lengths thus obtained. A nominal fuselage outside diameter of 16.4 feet was obtained with this seating arrangement. Fuel was stored under the passengers, with the tank shape optimistically assumed to conform to the shape of its confines (i.e., the cabin floor on the top and the bottom half of the fuselage walls for the rest of the circumference of a section). A space of 6 inches was allowed between the tank and floor and fuselage walls to accommodate insulation. A nominal under-floor tank cross-sectional area of 44.4 square feet was thus obtained. A cargo hold of 1200 cubic feet was also provided under the passengers. When the cargo and fuel tank cross sections are assumed to be the same, the cargo hold is found to be 27 feet long. After subtracting this length from the 140-foot length of the passenger cabin, an under-floor fuel volume of about 5000 cubic feet was estimated to be available. The aft body closure (some 60 ft in length) was assumed to be unavailable for tankage. The remainder of the fuel requirement was stored in cylindrical tanks aft of the passenger cabin and ahead of the aft closure (fig. 2). Fuselage length was varied as required with the length of the full-diameter tankage. The length of this tankage was determined by the equation

$$\ell_{H_2} = \frac{V_{H_2} - 6170}{186} \tag{2}$$

where 6170 is the number of cubic feet of liquid hydrogen carried in the wings and under the passengers and the denominator of 186 is the full-diameter fuselage tank cross sectional area in square feet. In figure 2, a fuel volume of 26 300 cubic feet is indicated. This corresponds to a fuel weight of 115 000 pounds, the amount (including reserves) ultimately found to be required for the nominal 4000-mile mission of this study. Equation (2) indicates that $\ell = 108$ feet for this case. The fuselage length can be obtained by adding the tank length ℓ_{H_2} to the fixed fore and aft lengths of the fuselage, as follows:

$$L_{fus} = 249 + \ell_{H_2} \tag{3}$$

After rewriting equation (2) in terms of fuel mass instead of volume and then substituting into equation (3), we get

$$L_{fus} = 216 + 0.001233\ W_{H_2} \tag{4}$$

The hydrogen-fuel airplane depicted in figure 2 thus needs a fuselage length of 358 feet for its 115 000-pound fuel load.

The fuel tank weight for the cryogenic fuels was estimated as

$$W_{tanks} = 0.383\ V_{fuel} \tag{5}$$

based on the weight and volume of a cylindrical tank reported in reference 11. Since all the tanks used in the airplane were not cylindrical, the weights computed with this equation may be somewhat optimistic. For the hydrogen airplane shown in figure 2, the tankage weight was computed to be 10 100 pounds.

Each tank was surrounded by insulation whose weight was assumed to be influenced by tank wetted area, the maximum radiating temperature of the surrounding surface, and the exposure time at this temperature. The airplane surface temperature at Mach 2.7 cruise is estimated to be 370° F (ref. 12). For this temperature, the insulation weight was calculated as

$$W_{insulation} = 0.32\ KS_{tanks} \tag{6}$$

where K is a function of cruise time as shown in figure 3. Both the coefficients and equation (6) are from refrence 13, although the data of figure 3 had to be extrapolated for durations greater than the maximum presented there. For the hydrogen-fueled airplanes, the tank wetted

area in square feet was estimated as

$$S_{H_2 tanks} = 5300 + 48.4\ \ell_{H_2} \tag{7a}$$

or

$$S_{H_2 tanks} = 0.0597\ W_{H_2} + 3692 \tag{7b}$$

By either equation, the tank wetted area of the hydrogen airplane of figure 2 is estimated to be 10 500 square feet. The cruise time at Mach 2.7 was calculated to be 8400 seconds. From figure 3, it is found that $K = 1.09$ for this cruise duration. The insulation weight is found to be 3660 pounds by substituting these values into equation (6). The total fuel tankage plus insulation weight, then, of the hydrogen airplane of figure 2 is approximately 13 800 pounds.

Methane-fuel tankage dimensions and weights. - Methane-fueled airplanes were handled in a manner similar to that just discussed for hydrogen fuel. Acceptable body length-to-diameter ratio was obtained, however, with six abreast, single-aisle seating. Only a small amount of fuel was stored in the wing with the rest being stored, as before, below and aft of the passengers.

A nominal body diameter of 13.0 feet was obtained with the six-abreast configuration. After allowing for 6 inches between the tank walls and fuselage floor and walls, the cross-sectional area of the under-floor tanks was found to be 18.1 square feet. A cargo hold 65 feet long was provided under the floor to accomodate 1200 cubic feet of cargo. A length of 27 feet was allowed for landing gear stowage. After making these allowances, a fuel storage volume of about 1000 cubic feet was available under the passenger cabin. The aft body closure (some 46 ft in length) was assumed to be unavailable for tankage. As before, the wing tanks were assumed to hold 1170 cubic feet of fuel. The remainder of the methane fuel was stored in 12-foot diameter cylindrical tanks between the passenger cabin and the aft closure. The length of this full-diameter fuselage tankage was found by the equation

$$\ell_{CH_4} = \frac{V_{CH_4} - 2170}{113} \tag{8}$$

The fuselage length can be obtained by adding the tank length thus computed to the fixed fuselage lengths ahead of and behind the full-diameter tanks, as follows:

$$L_{fus} = 237 + \ell_{CH_4} \tag{9}$$

By rewriting equation (8) in terms of mass instead of volume, and then substituting into equation (9), we obtain

$$L_{fus} = 218 + 0.000334\ W_{CH_4} \tag{10}$$

Fuselage lengths thus calculated are typically about equal to those of the JP-fueled airplanes with smaller body diameter.

Methane tankage and insulation weights are calculated as for hydrogen fuel by equations (5) and (6), respectively. For the methane-fueled airplanes, the tank wetted area was estimated as

$$S_{CH_4 tanks} = 2800 + 37.7\ \ell_{CH_4} \tag{11a}$$

or

$$S_{CH_4 tanks} = 0.01258\ W_{CH_4} + 2076 \tag{11b}$$

Empty weight variation with airplane dimensional and gross-weight changes. - Since takeoff gross weight was allowed to vary and was used as the figure of merit for the fixed-range and fixed-payload mission, it was necessary to make assumptions concerning the corresponding variation of empty weight. Not only is the empty weight influenced by variations in gross weight, but also by variations in the type and amount of fuel needed. This latter variation influences not only the previously discussed tankage and insulation weight, but also the fuselage dimensions and, therefore, weight. The equations which follow allow the estimation of major airframe component weights which are likely to be affected by dimensional and gross weight changes.

The wing weight was assumed to vary with both wing loading (i.e., W_g/S) and gross weight, as follows:

$$W_{wing} = 102\ 800 \left[\frac{60}{(W_g/S)} \times \left(\frac{W_g}{750\ 000} \right)^2 \right]^{0.64} \tag{12}$$

This equation is simply equation (1) with appropriate values from table II substituted for the reference wing weight, wing loading, and gross weight.

The fuselage weight was assumed to vary directly with diameter and length, as would be the case for a thin-walled hollow cylinder. Based on this premise and adjusting the coefficient to give the reference body weight of table II for those body dimensions (i.e., a length of 322 ft and a nominal diameter of 11.4 ft), the following equation was developed:

$$W_{fus} = 15.7\ D_{fus} L_{fus} \tag{13}$$

The weight of the tail was assumed to scale directly with wing area. After calculating a constant of proportionality based on the tail weight of table II and expressing wing area as the quotient of the gross weight divided by the wing loading, we have the expression

$$W_{tail} = 0.0752 \frac{W_g}{W_g/S} \tag{14}$$

Landing gear weight was maintained as a fixed percentage of the design takeoff gross weight. Based on this assumption and the landing gear weight of table II, we can express this weight as

$$W_{\ell g} = 0.49\ W_g \tag{15}$$

Propulsion system weight varied as a function of gross weight, wing loading, the engine design parameters, and the takeoff throttle setting. A further discussion appears later in the propulsion section. The remaining items comprising the operational empty weight (i.e., the weight of fixed equipment and the weight due to tolerance, standard and operational items, and airline options) are fixed throughout the study at the values indicated in table II.

Aerodynamics. - The drag polars used in this study were based on NASA-Langley Research Center data for a SCAT 15F-9898 (S_{wing} = 9898 ft^2) arrow-wing configuration. The data furnished by Langley consisted only of operational C_L's and C_D's occurring at intervals along a flight profile (fig. 1) for an airplane with a takeoff gross weight of 800 000 pounds. It was assumed for the purposes of this study that these coefficients would lie on parabolic drag polars described by the equation

$$C_D = C_{D_{min}} + \left[\frac{C_{D_i}}{\left(C_L - C_{L_o}\right)^2}\right]\left(C_L - C_{L_o}\right)^2 \tag{16}$$

Schedules of $C_{D_i} \Big/ \left(C_L - C_{L_o}\right)^2$ and C_{L_o} against Mach number were assumed, based on data available from earlier versions of the arrow-wing airplane. A value of $C_{D_{min}}$ was then computed from equation (16) for each C_L and C_D data pair with the assumed values of $C_{D_i} \Big/ \left(C_L - C_{L_o}\right)^2$ and C_{L_o}. The reference set of aerodynamic coefficients thus established is shown plotted against Mach number in figure 4.

In this study, however, we must change the relative wing, fuselage, and tail dimensions among airplanes (as is evident from the airplane sketches of fig. 2). Even for representative JP fuel airplanes of this study, the wing area is larger than the 9898-square-foot reference for the same gross weight while the fuselage dimensions are only slightly different. The drag polars must be adjusted from the reference values represented by the coefficients of figure 4 to account for these changes in relative component dimensions. Drag build-up curves showing the amount of drag accounted for by each component are needed before the effect of relative area changes can be determined. Unfortunately, these were not readily available.

The airframe component areas and dimensions for the reference 15F-9898 airplane were then estimated as a first step in the synthesis of a drag build-up procedure. The airframe was broken down into a set of components: wing, body, vertical tail, and horizontal tail. Total minimum drag from the reference polars was assumed to be composed of the sum of the friction and pressure, or wave, drags of these components. The nacelles were not considered as such, but an area representative of their surface area for a reference size was included with the body area.

The component skin friction coefficients were calculated by means of the Prandtl-Schlichting equation

$$C_{f_{component}} = \frac{0.455}{(\log_{10} Re_{component})^{2.58}} \tag{17}$$

This equation gives the skin friction coefficient for incompressible turbulent flow over one surface of a flat plate. These coefficients were then corrected for compressibility effects by a correction factor which was a strong function of Mach number and a weak function of altitude. These correction factors are based on empirical turbulent flow flat plate data (e.g., ref. 14) which vary with Reynolds number and Mach number. The total airplane friction drag coefficient, based on a reference wing planform area, was obtained by correcting the component skin friction coefficients to the common reference area and adding, as follows:

$$C_{D_{f_{total}}} = 2\left(C_{f_{wing}} + C_{f_{vt}} \times \frac{S_{vt}}{S_{wing}} + C_{f_{ht}} \times \frac{S_{ht}}{S_{wing}}\right) + C_{f_{body}} \times \frac{S_{body}}{S_{wing}} \tag{18}$$

The wing, vertical tail, and horizontal tail skin friction coefficients in this equation are doubled to account for both surfaces of these components.

The pressure drag coefficients of each of the various components based on a representative component area are corrected to the wing

planform area and added, as follows:

$$C_{D_{P_{total}}} = C_{D_{P_{wing}}} + C_{D_{P_{vt}}} \times \frac{S_{vt}}{S_{wing}} + C_{D_{P_{ht}}} \times \frac{S_{ht}}{S_{wing}} + C_{D_{P_{body}}} \times \frac{A_{body}}{S_{wing}} \tag{19}$$

The body and tail pressure drag coefficients based on their representative component areas are assumed to be scheduled with Mach number in the same manner as representative empirical data for these types of components in other airplanes. The wing pressure drag coefficient was varied in an iterative calculation at each Mach number until the total minimum drag coefficient obtained by adding equations (18) and (19) agreed with the reference $C_{D_{min}}$ (fig. 4).

In the equation representing the parabolic drag polars (eq. (16)), both the induced drag term within brackets and C_{L_o} were assumed to have a schedule against Mach number (top two curves of fig. 4) that did not change with variations of the relative component dimensions. The $C_{D_{min}}$ term will, however, vary as the body-to-wing area ratios in equations (18) and (19) change. (The area ratios between the tail components and the wing are assumed to remain constant in this study.) In addition, the skin friction coefficients of the wing, tail, and body components change because of changes in the characteristic length in the Reynolds number term of equation (17). The component pressure drag coefficients based on their own representative areas (eq. (19)) are assumed to have a fixed schedule with Mach number. Typical variations in $C_{D_{min}}$ resulting from this type of analysis are shown in figure 5 for two study airplanes. The reference $C_{D_{min}}$ schedule (fig. 4) from which these adjustments were made is also shown. The $C_{D_{min}}$ schedule of the hydrogen fuel airplane is higher than the reference schedule because the fuselage size increased while the wing size shrunk. (If they had changed at the same rate, there would have been only a small shift in the schedule due to the Reynolds number effect on the skin friction.) The $C_{D_{min}}$ schedule of the JP airplane is shifted downward because the fuselage did not grow at the same rate as the wing.

Engines

Duct-burning turbofans were selected as the engines for these study airplanes. Previous analyses (ref. 15) had shown that this engine type was most apt to benefit, in the presence of engine noise constraints,

from the higher turbine temperatures permitted by advanced cooling technology. Furthermore, the use of hydrogen fuel might permit still higher temperatures to be considered since the low temperature and greater heat sink of hydrogen fuel make it seem attractive as a coolant for the hot turbine parts. Turbine-inlet temperature as well as fan pressure ratio and bypass ratio were varied in this study. Overall fan-plus-compressor pressure ratio was fixed at a sea-level-static design value of 10 since the results of reference 15 indicated that this value was about optimum in the presence of a noise constraint for the range of turbine temperatures to be considered. The maximum duct burner temperature set for all engines was 2300° F. The duct burner was not lit in these studies until the transonic region was approached. Maximum burning was provided only up to the Mach 2.7 cruise condition. At this point, it was reduced to a level determined to be optimum by a maximization of the L/D over sfc quotient as initial cruise altitude was varied. In general, for the engines and airplanes of this study, these cruise duct-burner temperatures were in the vicinity of 1050° F.

Component matching and mode of operation. - Off-design performance calculations for these two-spool engines were made with the GENENG computer program (ref. 16). Fan, compressor, and high- and low-pressure turbine maps representing this class of engine were stored in the program on a non-dimensionalized basis to permit scaling as design parameters were changed. Basically, the computer program matches the fan and compressor with their driving turbines to satisfy requirements of flow continuity and power balance. For each set of engine design parameters, the primary nozzle throat area was varied to minimize sideline jet noise after lift-off (out of the ground effect) while still retaining the required thrust. The remainder of the performance was calculated with the primary nozzle area fixed at the sea-level-static design value. The duct nozzle throat area was floated as required as duct-burner temperature was varied throughout the mission. Variation of the primary nozzle throat area with the duct-burner unlit permitted a reduction of as much as 4 EPNdB in sideline noise at the required thrust level.

A summary of component characteristics at both takeoff and cruise for a representative study engine is shown in table III. Engines with other design fan pressure ratios, bypass ratios, and turbine rotor-inlet temperatures were considered in the study, but this engine is representative of a good design for sideline noise approximating that allowable by FAR 36. The exact duct-burner temperature used in cruise is a function of the airplane gross weight ultimately found to be required for the mission, as well as the engine size dictated by the takeoff thrust-to-gross-weight ratio requirement. The duct-burner temperature of 1040° F appearing in table III is for a JP-fuel airplane with a takeoff gross weight of 842 000 pounds and a lift-off thrust-to-gross weight ratio of 0.29. The corresponding sea-level-static corrected airflow is 1386 pounds per second for each of the four engines.

Weight. - Engine weights were obtained by the correlation technique of reference 17, based on weight technology that is two years more advanced than that of the GE4-J5P afterburning turbojet engine that had been proposed for the recent Boeing 2707-300 SST. Reference 17 provides an estimated weight of a turbofan engine without duct-burner, exhaust nozzle, and accessories. Neither does it account for the weight of inlet or nacelle. These items must be included to obtain the propulsion system weight of the four engines shown in table II. Propulsion system weights were first calculated for four 1000-pound-per-second engines. These weights were then scaled to the proper size (e.g., 1235 lb/sec in table II) by multiplying by the corrected airflow ratio raised to the 1.2 power (the scaling factor for the bare engine recommended in ref. 17). A weight breakdown follows for a propulsion system containing four 1000-pound-per-second duct-burning turbofans (BPR = 2, FPR = 3, OPR = 10, and $T_4 = 2725^\circ$ F):

Bare engines (ref. 17)	27 440 pounds
Duct burners and exhaust nozzles	24 600
Inlets and nacelles	21 500
Fixed installation	5 820
Total (four installed engines @ 1000 lb/sec each)	79 360 pounds

To obtain the weight shown in table II, the total installed weight was scaled with airflow, as follows:

$$\text{Propulsion system weight} = 79\,360 \times \left(\frac{1235}{1000}\right)^{1.2} = 102\,240 \text{ lb}$$

Fuel type. - Engines having identical design parameters were generally assumed to deliver the same thrust and have the same weight, regardless of the fuel type. The specific fuel consumption was taken to vary inversely as the fuel heating value. The error in sfc due to this assumption is small (ref. 18). Studies at NASA-Lewis in the 1950's suggested that hydrogen fuel would permit shorter combustors and, hence, lighter engines. However, modern JP combustors are shorter than those of that time period, and it was not possible in this preliminary study to estimate whether hydrogen would offer any further advantage. Conversely, the weight of any heat exchangers that might be added for the cryogenic systems was also ignored.

Turbine cooling. - Compressor discharge air was bled around the primary combustor to cool both the high- and low-pressure turbines. Bleed air requirements for blade metal temperatures of 1750° F and vane metal temperatures of 1850° F were calculated by using the full-coverage-film-cooling curve of reference 19. The high-pressure turbine was assumed to consist of a single stage while the low-pressure turbine was assumed to consist of three stages for all the study engines. The cooling requirement is most severe at the Mach 2.7 condition because the cooling air coming from the compressor discharge is just over 1000° F for all engines

(since they all have an overall fan-plus-compressor pressure ratio of 10). According to reference 20, a stage bleed flow of 3 percent is in the middle of the usable range. Accordingly, this value was chosen for the first stage (high-pressure) rotor of the reference engine, exclusive of wall and shroud considerations. A cooling effectiveness of 0.565 was obtained for this amount of bleed from the curve of reference 19 for the first stage rotor. The definition of cooling effectiveness yields a rotor-inlet temperature of 2725° F when the metal temperature is 1750° F and the coolant temperature is 1000° F. Bleed requirements for each succeeding stage (both stator and rotor) were calculated in a similar manner. The stage cooling flow computed by this method was multiplied by 1.33 to account for cooling the shroud and wall in addition to the blade or vane. The total cycle chargeable cooling flows thus obtained were typically about 10.5 percent of the compressor discharge air (see table III) for the engines with a turbine rotor-inlet temperature of 2725° F. (High-pressure turbine stator cooling is not cycle chargeable.)

As mentioned previously, engine performance was assumed to remain unchanged with a change in fuel type with the exception of sfc which was assumed to be inversely proportional to the heating value. But because of the lower temperature and greater heat sink of hydrogen fuel, less turbine cooling bleed may be required for any given turbine inlet temperature than with JP fuel. To account for this possibility, some cases were computed for hydrogen with no cooling bleed. At the rotor-inlet temperature of 2725° F, the difference in the gross weight of a hydrogen-fueled airplane with 10.5 percent chargeable bleed and no chargeable bleed is almost undetectable.

Sizing. - The engine size (i.e., design airflow) was selected to give sufficient thrust (duct burner unlit) for an FAR takeoff field length not to exceed 12 400 feet on a +15° C day and also achieve an altitude of 1500 feet at 3.5 miles from brake release. (The latter condition should provide sufficient margin on flyover community noise as per FAR 36 so that after power cutback it is less than sideline noise; alternatively, climb rate beyond 3.5 n.mi. can be increased above the minimum set by FAR 36 to provide 108 EPNdB at the 3.5-mile station with a reduced noise footprint.) For the airplanes in this study having a takeoff wing loading of 60 pounds per square foot (the value chosen as optimum in ref. 9 for turbojet-powered airplanes of this type using JP fuel), a lift-off thrust-to-gross weight ratio of about 0.29 is estimated to be required for the above conditions. The duct-burner was unlit during takeoff with the turbine temperature at its design value. Primary exhaust nozzle throat area was adjusted as required for each set of engine design parameters to minimize sideline jet noise with the least thrust penalty. Jet noise out of ground effect (i.e., without any extra ground attenuation) and without any benefit of fuselage masking of two of the engines was calculated at the FAR 36 sideline distance of 0.35 nautical miles using the standard SAE technique (refs. 21 and 22).

Installation. - An inlet pressure recovery schedule similar to that of the Boeing 2707-300 (ref. 23) was used in these engine performance calculations. (Sea-level-static and Mach 2.7 values of this parameter are shown in table III.) Variable inlet geometry was assumed to provide external compression at speeds up to Mach 1.6 with the centerbody fully extended. Beyond Mach 1.6 the centerbody was fully retracted for external-internal compression. No secondary airflow from the inlet was assumed for the exhaust nozzles used in this study. The nozzle thrust coefficients used in these calculations for both the primary and the duct nozzles were fixed at a value of 0.98 for all flight conditions. Inlet drag, including spillage, bypass, and bleed effects, was also accounted for in the engine performance calculations. At Mach 2.7, there was no spillage or bypass; inlet drag consisted entirely of that due to dumping boundary layer bleed air. During cruise at Mach 2.7, engine airflow was unchanged from its full power value. The inlet drag during cruise, therefore, was independent of power setting. During full-power supersonic climb and acceleration, spillage was the dominant component of inlet drag up to about Mach 2.2.

Installed engine performance is shown in figure 6 at supersonic cruise and subsonic hold for representative JP- and hydrogen-fueled engines of 1000 pound-per-second size. This performance data is for a duct-burning turbofan having a sea-level-static design bypass ratio of 2, fan pressure ratio of 3, overall fan-plus-compressor pressure ratio of 10, turbine rotor-inlet temperature of 2725° F, and a maximum duct-burner temperature of 2300° F. For supersonic cruise, the optimum cruise altitude is not really known until the engine is "flown" in an airplane on a simulated mission. Supersonic cruise performance, therefore, is plotted for several altitudes (fig. 6(a)). The circled points at the right of each curve represent maximum duct burning while the square points at the left represent the maximum dry (non-duct-burning) thrust. The minimum sfc occurs at a duct-burner temperature of about 1050° F. (With duct-burner unlit, the duct temperature is 684° F at the Mach 2.7 condition.) Because of the takeoff sizing constraints and the optimization of the Breguet cruise altitude, both the JP- and hydrogen-fuel engines of this study typically cruise at a thrust setting near the bucket of these and similar performance curves. The Reynolds number variation with altitude, which would have only a small effect over this range of altitudes, has been ignored in constructing these curves.

For subsonic hold performance (fig. 6(b)), the part-power performance curve is shown for each fuel only over the thrust range of interest. Maximum thrust would be about 29 300 pounds (with duct burner unlit). For the optimized JP-fueled airplanes of this study, the hold specific fuel consumption was generally about 1.1 pounds of fuel per hour per pound of thrust. For the hydrogen-fuel airplanes, the throttle setting is higher - near the right-hand end of the curve (fig. 6(b)). The corresponding sfc (0.34 lb/hr/lbf) is even lower, therefore, than a mere correction of the JP-fuel sfc by the heating value ratio would indicate. This difference in throttle setting is the result of the hydrogen-fuel airplane having a

higher operating-empty weight fraction than the JP airplane. (During hold, the airplane weight almost equals the operating empty weight.) No turbine cooling bleed was used for the range of throttle settings shown in figure 6(b) because the turbine rotor-inlet temperature was below 1750° F. Methane performance is not shown in figure 6, mainly to prevent crowding of the JP curves. Methane sfc can easily be obtained at any thrust level by multiplying the JP sfc by the ratio of the JP heating value to the methane heating value (from table I).

RESULTS AND DISCUSSION

Wing Loading

Prior to the main study, wing loading was varied for both JP- and hydrogen-fuel airplanes in order to determine the optimum values for use in the rest of the analysis. The takeoff gross weight was fixed at 850 000 pounds for JP and 500 000 pounds for hydrogen in this part of the study. These gross weights were selected to give ranges near 4000 nautical miles - the range selected as the design for the main part of the study. Payload was fixed at 250 passengers. Range was then allowed to vary as the figure of merit as wing loading was changed. The results of this optimization show (fig. 7(a)) that the best wing loading for either fuel is 60 pounds per square foot when unsuppressed duct-burning turbofan engines are used (with takeoff at the maximum dry setting). The JP result agrees with the results found in a previous study with noise-constrained dry turbojet engines installed in a similar arrow-wing airplane (ref. 9). Since the methane airplane results are expected to lie between those for JP and hydrogen, it is assumed that its optimum wing loading will also be 60 pounds per square foot.

Not only is the wing size becoming smaller as wing loading is increased, but the fuselage of the hydrogen-fuel airplane is being lengthened somewhat to accommodate the additional fuel that is required to maintain a constant gross weight (fig. 7(b)). The JP fuselage dimensions remain constant, of course, as design fuel load varies.

Figure 7(c) shows how the supersonic cruise lift-drag ratio decreases as wing loading is increased for both the JP- and hydrogen-fuel airplanes. The propulsion system weight must increase as wing loading is increased (fig. 7(d)) because the takeoff thrust requirements are more severe with smaller wings. The wing weight, however, as shown in figure 7(e), decreases with increasing wing loading. The wing weight for both fuels decreases faster than the propulsion system weight increases for a net favorable weight effect. Some further benefit is obtained from the decrease in tail weight as wing loading is increased. There is a trade occurring, then, between the unfavorable effect of a decreasing lift-drag ratio and the favorable effect of a lower empty weight. Also involved in the optimization is a slight change in cruise sfc which occurs as wing loading is

changed. This is very minor, however, because of the flatness of the bucket of the sfc-against-thrust curves (fig. 6(a)), and the fact that initial cruise altitude is re-optimized as wing loading is changed. Operation is always very near the minimum sfc point on these cruise performance curves.

The takeoff thrust requirement increases as wing loading increases (fig. 8(a)) when a 1500-foot altitude is specified for a point 3.5 nautical miles from brake release. For arrow wing airplanes having a 60-pound-per-square-foot wing loading, this lift-off thrust-to-gross-weight ratio is approximately 0.29. The lift-off Mach number (fig. 8(b)) rises as wing loading is increased if the lift-off C_L and, hence, angle of attack, is fixed. FAR takeoff field length also rises as wing loading is increased until, at a wing loading of 80 pounds per square foot, it has almost reached the permissible limit of 12 400 feet. An FAR field length of 10 300 feet is obtained at the optimum wing loading of 60 pounds per square foot. All the takeoff performance data plotted in figure 8 is extracted from reference 9. It is based on a simplified solution of the takeoff problem and is, therefore, only approximate. The trends illustrated, however, are probably accurate.

Engine Jet Noise

No noise suppressor. - In figure 9 the impact of the sideline noise on gross weight is presented for all three fuel types. Takeoff wing loading is fixed at the optimum value of 60 pounds per square foot. All airplanes were designed for the 4000-nautical-mile mission with a payload of 250 passengers. Data is presented for two engine cycles - both duct-burning turbofans with fan pressure ratios of 3, overall fan-plus-compressor pressure ratios of 10, and turbine rotor-inlet temperature of 2725° F. The solid curves on the right for both JP and hydrogen are for a design bypass ratio of 2.0, while the solid curves on the left are for a bypass ratio of 2.5. The circled points anchoring each solid curve represent takeoff with maximum dry thrust (i.e., design T_4 with duct-burner unlit). Points on each solid curve to the left of the circled points represent takeoff at less than maximum dry thrust with larger engines. Each point on these curves has had the primary nozzle throat area optimized at lift-off for minimum noise. The dashed curves connecting the circled points represent an approximate minimum gross weight envelope that can be obtained for each fuel type. A further optimization indicates that very little lowering of this envelope occurs as takeoff duct-burner temperature is optimized. These further studies indicate that at the FAR 36 noise level a slight amount of duct burning is optimum but will result in the gross weight being lowered by only about 1.2 percent for JP fuel.

Figure 9 shows that, at any specific noise level, there is a saving in gross weight by going to methane fuel and an even greater saving with hydrogen. Furthermore, the gross weight saving is even greater as noise

level is reduced. The gross weight of a hydrogen airplane is less sensitive to the possibility of lower noise requirements than is a JP airplane.

A further conclusion to be drawn from the curves of figure 9 is that it is better to re-optimize the engine design parameters to obtain a noise reduction than it is to throttle back with engine oversizing. The envelope curves have been replotted and extended to 102 EPNdB in figure 10 for JP and hydrogen. The FAR 36 noise limit (with possible 2 EPNdB noise trades neglected) is also shown. In general, as we proceed to the left on these curves, bypass ratio is increasing and fan pressure ratio is decreasing. For example, the point at 103 EPNdB on the JP curve is for an engine with a fan pressure ratio of 2.5 and a bypass ratio of 3.2. The gross weight penalty for lower noise is seen to become quite severe for JP fuel near the left-hand end of the curve.

With noise suppressor. - Jet noise suppressors having the characteristics shown in figure 11 were applied to the engines with a bypass ratio of 2.0 from figure 9. A gross thrust loss of 7.5 percent (0.5 percent per EPNdB of maximum suppression) was assumed for each of the two streams but no weight penalty was imposed. In general, suppression was different for the primary and duct streams because their exit velocities were unequal (primary stream velocity was greater than that of the duct). As shown in figure 12, the maximum dry takeoff power setting now yields sideline noise approximating FAR 36 minus 10 EPNdB. The gross weights of figure 12 are higher than the corresponding values from figure 9 not because of a suppressor weight penalty because there was none; the weight increase is due to an increase in the engine size which is needed to obtain adequate takeoff thrust after allowing for the suppressor thrust loss. Further weight increases in some of the airframe components (e.g., the wing and landing gear) must then be allowed to handle the added gross weight due to the larger engines. This gross weight increase necessitates still larger engine sizes and, hence, higher gross weights. So there can be a considerable amplification from the engine weight increment needed to overcome suppressor thrust loss to the gross weight ultimately found after several iterative calculations. Of course, the gross weights indicated in figure 12 are highly optimistic since no suppressor weight penalty was included. Because of the multiplier effect from an engine hardware weight increment, it is expected that realistic suppressor weight assumptions would considerably raise the gross weights from the levels shown in figure 12 - especially for JP fuel.

A comparison of figures 9 and 12 further reveals that the advantages of hydrogen fuel are greater at the suppressed FAR 36 minus 10 EPNdB noise level than they were without suppressors at FAR 36. At the lower noise level, figure 12 shows that the gross weight of a hydrogen airplane is only 55 percent of that for JP. Figure 9 shows that the hydrogen airplane weight is 60 percent at FAR 36.

In the remainder of the report, only unsuppressed cases will be considered.

Turbine Rotor-Inlet Temperature

Turbine rotor-inlet temperature T_4 was raised beyond the reference value of 2725° F for both JP and hydrogen fuel to determine the possible gross weight reduction, if any. At first, cycle-chargeable bleed was fixed at the reference 10.5-percent value as temperature was raised to obtain an optimistic appraisal of the benefits of higher temperature if better cooling and/or materials are postulated as occurring simultaneously with advances in temperature. Bypass ratio was increased as T_4 was raised in order to keep the core nozzle exit velocity constant. Fan pressure ratio was fixed at a value of 3 and the duct-burner was unlit at takeoff so that the duct exit velocity was constant. The total jet noise of the two streams, therefore, remained practically constant as T_4 was varied. The solid curves of figure 13 show how the takeoff gross weight varies as T_4 is increased for both JP and hydrogen when cooling bleed is constant. The lowest gross weight is achieved at T_4 = 3100° F with JP fuel for these optimistic bleed assumptions, but it is only 1.2 percent below the gross weight obtained at the reference temperature of 2725° F. When bleed is increased as T_4 rises, as required for constant cooling and materials technology, the gross weight is observed to increase (dashed curve, fig. 13). Hence, the 2725° F value of T_4, selected as the reference, was optimum for JP fuel when cooling was scheduled with temperature in a realistic manner.

The lower curve for hydrogen (fig. 13) shows that there is again no significant advantage to higher T_4 even when cooling bleed remains constant. It was assumed in the hydrogen-fuel calculations, in order to expedite them as much as possible, that cooling bleed equalled the reference JP value of 10.5 percent. Actually, however, the bleed flow could be considerably reduced for hydrogen fuel if its high heat sink and low temperature are used for cooling the turbine blades, either directly or indirectly as a heat sink for the bleed air. To examine the impact of this situation, with no heat exchanger weight penalty, a case was run at the reference T_4 with no cooling bleed. The result, indicated by the circled point in figure 13, shows that even the complete elimination of cooling bleed has little effect on takeoff gross weight.

Figure 14 shows how bypass ratio was scheduled against turbine temperture in order to keep the nozzle exit velocities constant. The solid curve is for the constant bleed situation while the dashed curve is for the realistic bleed schedule with constant technology.

Past studies (e.g., ref. 15) have usually indicated some advantage for higher T_4, especially when there was no noise constraint. These results, for JP fuel at least, will be influenced by the way cooling bleed

is scheduled with T_4. The results of figure 13, however, suggested that at the lower bleed flow requirements for hydrogen this scheduling has little influence on gross weight. Hydrogen-fuel airplanes were thus selected to examine the effect of higher T_4 when the noise constraint was not observed. A constant bleed flow was assumed with bypass ratio scheduled against T_4 as shown by the solid curve of figure 14. The maximum duct-burner temperature of 2300° F was maintained at takeoff. These results are shown in the lower curve of figure 15. The upper curve is the maximum dry takeoff curve from figure 13, presented here for comparison. The bottom curve with maximum duct burning and no noise constraint indicates that higher T_4's are desirable up to about 3300° F.

Example Airplanes

Based on the preceding figures, three comparably designed airplanes have been defined for the three fuels. Each airplane performs the same mission and meets the FAR 36 noise limit (if a 2-EPNdB trade is permitted) without suppressors. The engines in all cases are duct-burning turbofans with a bypass ratio of 2, fan pressure ratio of 3, and T_4 of 2725° F.

Weights appear in table IV with other pertinent characteristics in table V. Hydrogen permits a three-fold reduction in fuel weight, with a resulting 40-percent reduction in takeoff gross weight, and a 20-percent reduction in empty weight, compared to JP. The benefits of methane are much more modest.

Direct Operating Cost

A better measure of excellence than weight for a commercial vehicle is cost. The standard 1967 Air Transport Association formula (ref. 24) was used to compute DOC for the three example airplanes. For all fuels the specific airframe cost was taken as $178 per pound and the engine cost as $200 per pound. This is perturbed later.

Results are shown in figure 16 for a particular set of fuel costs: JP at 1.65 cents per pound (11 cents/gal), which had been a typical price until recent increases; methane at 1.60 cents per pound, based on an unpublished mid-1960's study by the Institute of Gas Technology; and hydrogen at 10 cents per pound, which is at the lower end of recent estimates of the potential for large-scale production of electrolytic hydrogen (e.g., ref. 25). Expressed in consistent units of cents per million Btu of energy, these costs are 89, 75, and 194, respectively.

The resultant DOC's are seen to be rather similar under these assumptions, with methane enjoying a slight advantage over JP, and hydrogen a slight penalty. If these differences were real, they would be quite significant to an airline. For example, a DOC difference of only

0.1 cent/seat-mile corresponds to $500 million per year for a fleet of 500 supersonic transports. However, it is not felt that the present study can significantly distinguish differences of these magnitudes.

One of the main cost uncertainties is the price of the fuel as delivered onboard the aircraft, considering that new cryogenic fueling facilities would have to be established at major airports around the world, probably with double lines for chill-down of hot airplane tanks, liquefaction plants to reliquefy vented vapor, helium purge provisions, special techniques to prevent condensing ambient water vapor or even the air itself on the cold surfaces, stringent safety precautions, etc.

The fly-away cost of liquid methane and hydrogen is thus very debatable. So too, however, is that of JP fuel as we look forward to a future time of shortages, greater dependence on unstable foreign suppliers, and inflation. Current price has already risen to 16 cents per gallon (ref. 26). The effect of variations in fuel cost on DOC is shown in figure 17. If the hoped-for reduction in hydrogen cost is not realized but instead turns out to cost 400 cents per million Btu (which, even so, is cheaper than today's price), then the DOC is nearly twice that of JP.

A further factor is that the hardware and maintenance cost of cryogenic systems is apt to be considerably higher than a JP system. The dashed line of figure 17 shows the effect of a 50-percent higher unit cost for all structure of the hydrogen airplane. Some parts of an airplane are entirely unaffected by fuel type, of course, while other parts may see some effect even though they are not directly in contact with the fuel. The 50-percent value is entirely arbitrary, just to display the possible importance of this factor. It is interesting to note that, with the 50-percent penalty, hydrogen and JP would have nearly equal DOC if the energy costs were to become the same at some future date.

Perturbations

Range. - It is generally the case that the benefits of the better heating value of the cryogenic fuels are magnified as the mission is made more demanding. Figure 18(a) shows how longer range increases the gross weight of the JP airplane faster than the hydrogen airplane. The corresponding DOC's are shown in figure 18(b). Depending on fuel cost, there is a break-even range beyond which hydrogen becomes superior.

Aerodynamic efficiency. - Another way to make the mission more challenging is to postulate less advanced technology. Figure 19 shows the effect of reducing the cruise lift-drag ratios by various amounts, starting from the previously obtained values of 9.85 for JP and 7.53 for hydrogen. As these values are reduced by the same percentages, a cross-over again occurs beyond which hydrogen becomes increasingly superior.

CONCLUDING REMARKS

A preliminary study has been made of the performance and operating cost of a representative Mach 2.7 supersonic transport when fueled by JP, methane, or hydrogen. The higher heating values of the cryogenic fuels, especially hydrogen, lead to major reductions in fuel weight and takeoff gross weight. No further benefit was found when the FAR 36 noise constraint was observed, however, by applying the cooling capacity of the cryogenic fuels to obtain turbine-rotor-inlet temperatures higher than the 2700° to 2800° F that was optimum for JP.

Using optimistically low values for hydrogen fuel cost and recent fossil-fuel costs, the direct operating cost of the methane airplane is slightly better than JP, while hydrogen is slightly worse. (No increase in airplane hardware price was included for the additional complexity of handling cryogenic fuels.) However, if the mission is made more demanding (e.g., in terms of engine noise, range, or less advanced technology), hydrogen suffers less than the other fuels and so becomes relatively more desirable. It may be postulated that, because of future increases of JP and methane costs and/or reductions in hydrogen cost, the condition will be approached where all fuels have equal costs per unit of energy content. If such is the case, then direct operating cost will be about 20 percent lower for hydrogen than for JP on the reference mission. But it must be recognized that the difficulties of developing and operating cryogenic ground facilities, engines, and airframes may incur direct and indirect costs that have not been addressed in this paper.

A more refined study including technology problems and safety for both the ground and airborne systems must thus be made to properly assess the merits of the cryogenic fuels. This statement implies that the designer has some choice of fuel type. If the situation is envisioned where fossil fuels are exhausted, then it appears that hydrogen will be a very adequate substitute fuel for supersonic transports after the practical problems have been solved.

APPENDIX - SYMBOLS

A	cross-sectional area, ft^2
BPR	bypass ratio
C_D	drag coefficient
C_f	friction coefficient
C_L	lift coefficient
C_{L_o}	lift coefficient where $C_{D_{min}}$ occurs
D	drag, lb
D_{fus}	fuselage nominal diameter, ft
DBTF	duct-burning turbofan engines
DOC	direct operating cost, cents/seat-statue-mi
F_n	net thrust, lb
FAR	Federal Air Regulation
FPR	fan pressure ratio
H-P	high-pressure (turbine)
K	insulation weight time correction factor
L	lift, lb
L_{fus}	fuselage length, ft
ℓ	length of full-diameter fuselage tanks, ft
L-P	low-pressure (turbine)
OPR	overall fan-plus-compressor pressure ratio
Re	Reynolds number at free-stream conditions
S	projected wing or tail planform area or body or fuel tank surface area, ft^2
sfc	specific fuel consumption, lb/hr of fuel per lb of net thrust
SLS	sea-level, static

TOGW takeoff gross weight, lb

T_4 turbine rotor-inlet temperature, $^{\circ}F$

V total fuel volume, ft^3

W weight, lb

Subscripts:

f friction

g gross, takeoff

ht horizontal tail

i induced, due to lift

ic incompressible flow

min minimum

p pressure or wave

ref reference

vt vertical tail

REFERENCES

1. Silverstein, Abe; and Hall, Eldon W.: Liquid Hydrogen as a Jet Fuel for High-Altitude Aircraft. NACA RM E55C28a, 1955.

2. Lewis Laboratory Staff: Hydrogen for Turbojet and Ramjet Powered Flight. NACA RM E57D23, 1957.

3. Weber, Richard J.: Propulsion for Hypersonic Transport Aircraft. Proceedings of the Fourth Congress of the International Council of the Aeronautical Sciences. R. R. Dexter, ed. Spartan Books, Inc., 1965, pp. 977-999.

4. Becker, John V.: Prospects for Actively Cooled Hypersonic Transports. Astronautics and Astronautics, vol. 9, no. 8, Aug. 1971, pp. 32-39.

5. Williams, Laurence O.: The Cleaning of America. Astronautics and Aeronautics, vol. 10, no. 2, Feb. 1972, pp. 42-51.

6. Gregory, D. P.; and Wurm, J. E.: A Hydrogen Energy System. Presented at the Conference on Natural Gas Research and Technology, Atlanta, Ga., June 5-7, 1972.

7. Weber, Richard J.; Dugan, James F., Jr.; and Luidens, Roger W.: Methane-Fueled Propulsion Systems. Astronautics and Aeronautics, vol. 4, no. 10, Oct. 1966, pp. 48-55.

8. Whitlow, John B., Jr.; and Kraft, Gerald A.: Potential of Methane-Fueled Supersonic Transports Over a Range of Cruise Speeds up to Mach 4. NASA TM X-2281, 1971.

9. Whitlow, John B., Jr.: Comparative Performance of Several SST Configurations Powered by Noise-Limited Turbojet Engines. NASA TM X-68178, 1972.

10. Struck, H. G.; and Butsko, J. E.: Booster Wing Geometry Trade Studies. NASA Conference, Vol. I. NASA TM X-2272, 1971, pp. 611-642.

11. Heathman, John H.: Hydrogen Tankage Application to Manned Aerospace Systems. Phases II and III. Vol. I. Design and Analytical Investigations. Rep. GDC-DCB68-008-Vol. 1, General Dynamics/Convair (AD-83323), Apr. 1968. (Available to qualified requestors from DDC; Others from Air Force Flight Dynamics Lab., Attn: FBS, Wright-Patterson AFB, OH 45433.)

12. Sutcliffe, P. L.: The General Problem. Supersonic Engineering. J. T. Henshaw, ed., John Wiley & Sons, Inc., 1962, pp. 1-17.

13. Thompson, W. R.: Weight and Size Analysis of Advanced Cruise and Launch Vehicles. Vol. I: Final Technical Report and Data Handbook. Rep. GDC-DCB-66-008, Vol. 1, General Dynamics/Convair (NASA CR-89451), Feb. 1966.

14. Matting, Fred W.; Chapman, Dean R.; Nyholm, Jack R.; and Thomas, Andrew G.: Turbulent Skin Friction at High Mach Numbers and Reynolds Numbers in Air and Helium. NASA TR R-82, 1961.

15. Koenig, Robert W.; and Kraft, Gerald A.: Influence of High-Turbine-Inlet-Temperature Engines in a Methane-Fueled SST when Takeoff Jet Noise Limits Are Considered. NASA TN D-4965, 1968.

16. Koenig, Robert W.; and Fishbach, Laurence H.: GENENG - A Program for Calculating Design and Off-Design Performance for Turbojet and Turbofan Engines. NASA TN D-6552, 1972.

17. Gerend, Robert P.; and Roundhill, John P.: Correlation of Gas Turbine Engine Weights and Dimensions. Paper 70-699, AIAA, June 1970.

18. Wilcox, E. Clinton; Weber, Richard J.; and Tower, Leonard K.: Analysis of of Turbojet and Ramjet Engine Cycles Using Various Fuels. NACA RM E56I19a, 1956.

19. Livingood, John N. B.; Ellerbrock, Herman H.; and Kaufman, Albert: 1971 NASA Turbine Cooling Research Status Report. NASA TM X-2384, 1971.

20. Denning, R. M.; and Hooper, J. A.: Prospects for Improvement in Efficiency of Flight Propulsions Systems. J. Aircraft, vol. 9, no. 1, Jan. 1972, pp. 9-15.

21. Anon.: Jet Noise Prediction. Aerospace Information Rep. 876, SAE, July 10, 1965.

22. Anon.: Definitions and Procedures for Computing the Perceived Noise Level of Aircraft Noise. Aerospace Recommended Practice 865, SAE, Oct. 15, 1964.

23. Anon.: Boeing's Latest SST Proposal. Part One. Flight International, vol. 95, no. 3123, Jan. 16, 1969, pp. 104-108.

24. Anon.: Standard Method of Estimating Comparative Direct Operating Costs of Turbine Powered Transport Airplanes. Air Transport Assoc. of America, Dec. 1967.

25. Alexander, Arthur D.: Economic Study of Future Aircraft Fuels (1970 - 2000). NASA TM X-62180, 1972.

26. Anon.: Jet Fuel Prices Rising in Europe. Aviation Week & Space Tech., vol. 98, no. 4, Jan. 22, 1973, p. 19.

TABLE I. - FUEL PROPERTIES AND PROPERTIES RELATIVE TO JP FUEL

(a) Fuel properties

Type	HV, (Btu/lb)	Heat sink, Btu/lb at ^{o}F		Density, lb/ft^3	B.P., ^{o}F
JP	18 500	365	700	50	300
M	21 500	1100	1000	26.5	-259
H_2	51 500	4900	1000	4.4	-423

(b) Relative fuel properties

Type	HV, (Btu/lb)	Cool. capacity (Btu/flow rate)	Tank volume	Relative cost	at ¢/lb
JP	1	1	1	1	1.65
M	1.16	2.6	1.6	0.83	1.60
H_2	2.78	4.8	4.1	2.18	10

TABLE II. - COMPONENT WEIGHTS OF REFERENCE JP-FUEL MACH 2.7 ARROW-WING AIRPLANE

[TOGW = 750 000 lb, 250 seats]

Component	Weight, lb
Wing (S = 12 500 ft^2)	102 800
Tail	9 400
Body	57 680
Landing gear	36 700
Fixed equipment	62 530
Tol., std. and opt. items	15 300
Propulsion system	102 240
Operational empty wt (OEW)	386 650

TABLE III. - COMPONENT CHARACTERISTICS OF A REPRESENTATIVE DUCT-BURNING TURBOFAN ENGINE USED IN THIS STUDY

Characteristic	Mach number/Power setting	
	0/Takeoff	2.7/Cruise
Inlet pressure recovery	0.960	0.916
Corrected L-P shaft speed, percent design	100	66.4
Actual L-P shaft speed, percent design	100	90.1
Corrected H-P shaft speed, percent design	100	87.9
Actual L-P shaft speed, percent design	100	109.0
Corrected airflow at fan face, percent design	100	60.6
Fan pressure ratio	3.00	1.74
Inner compressor pressure ratio	3.33	2.31
Bypass ratio	2.00	2.36
Fan adiabatic efficiency, percent	85.0	82.5
Inner compressor adiabatic efficiency, percent	87.0	85.3
Horsepower extraction per 1000 lb/sec SLS airflow	133	133
Turbine rotor inlet temperature, ^{o}F	2725	2725
Pressure ratio across primary burner	0.944	0.935
Primary combustor efficiency, percent	0.985	0.985
Duct-burner temperature, ^{o}F	283	1040 (typical)
Duct-burner efficiency, percent	D/B unlit	0.930
Pressure ratio across duct burner	0.940	0.936
Cycle chargeable turbine cooling bleed, percent coreflow	10.5	10.5
Part of cooling bleed for H-P turbine, percent	34.8	34.8
Part of cooling bleed for L-P turbine, percent	65.2	65.2
H-P turbine adiabatic efficiency, percent	90.0	89.5
L-P turbine adiabatic efficiency, percent	90.0	90.0
Tailpipe pressure loss (core stream), $\Delta P/P$	0.02	0.02
Nozzle gross thrust (velocity) coefficient	0.98	0.98
Primary nozzle total temperature, ^{o}F	1753	1773
Primary nozzle pressure ratio (complete expansion)	1.851	16.2
Duct nozzle pressure ratio (complete expansion)	2.707	34.7

TABLE IV. - SST WEIGHT BREAKDOWN (POUNDS)

[DBTF engines without suppressors; max. dry takeoff for ~ FAR 36 noise; BPR = 2, FPR = 3, OPR = 10, T_4 = 2725° F, $T_{D/B\ max}$ = 2300° F; range = 4000 n.mi.; 250 passengers.]

	JP	CH_4	H_2
Wing	119 000	105 200	61 250
Tail	10 660	9 600	6 280
Body	57 680	65 220	92 200
Fuel tanks, insulation	0	6 450	13 760
Landing gear	41 300	37 500	24 500
Fixed equipment	62 530	62 530	62 530
Tol., std. and opt. items	15 300	15 300	15 300
Inlets, nacelles	40 400	38 100	21 700
Airframe weight	346 870	339 900	297 520
Engines and access. (inc. nozz., T.R.)	77 200	72 900	41 300
Operating empty weight	424 070	412 800	338 820
Payload (250 pass. and bagg.)	50 000	50 000	50 000
Total fuel (incl reserves)	397 930	302 200	115 180
Takeoff gross weight	842 000	765 000	504 000

TABLE V. - MACH 2.7 SST CHARACTERISTICS

[DBTF engines without suppressors; max. dry takeoff for ~ FAR 36 noise; BPR = 2, FPR = 3, OPR = 10, T_4 = 2725° F, $T_{D/B\ max}$ = 2300° F.]

	JP	CH_4	H_2
Takeoff gross wt, lb	842 000	765 000	504 000
Range, n.mi.	4000	4000	4000
Number of passengers	250	250	250
Wing planform area, ft^2	14 050	12 750	8 400
M2.7 CR. L/D/sfc, hr^{-1}	9.9/1.54	9.3/1.32	7.5/0.557
Cruise altitude, ft	66 000	66 500	66 500
Number of seats abreast	5	6	7
Number of aisles	1	1	2
Fuselage nom. O.D., ft	11.4	13.0	16.4
Fuselage length, ft	322	319	358
Fuel tank volume, ft^3	7400	11 400	27 400
Cargo volume, ft^3	1200	1200	1200
Sideline noise, EPNdB	110.0	109.7	108.4
Lift-off $F/F_{max\ dry}$, %	100	100	100
Lift-off $F_{max\ dry}/W_G$	0.29	0.29	0.29
Airflow per engine, lb/sec	1386	1262	830
Airframe/engine cost, $/lb	178/200	178/200	178/200
Fuel cost, cents/lb	1.65	1.60	10.00
cents/10^6 Btu	89	75	194
DOC, cents/seat-st.mi.	1.52	1.39	1.68

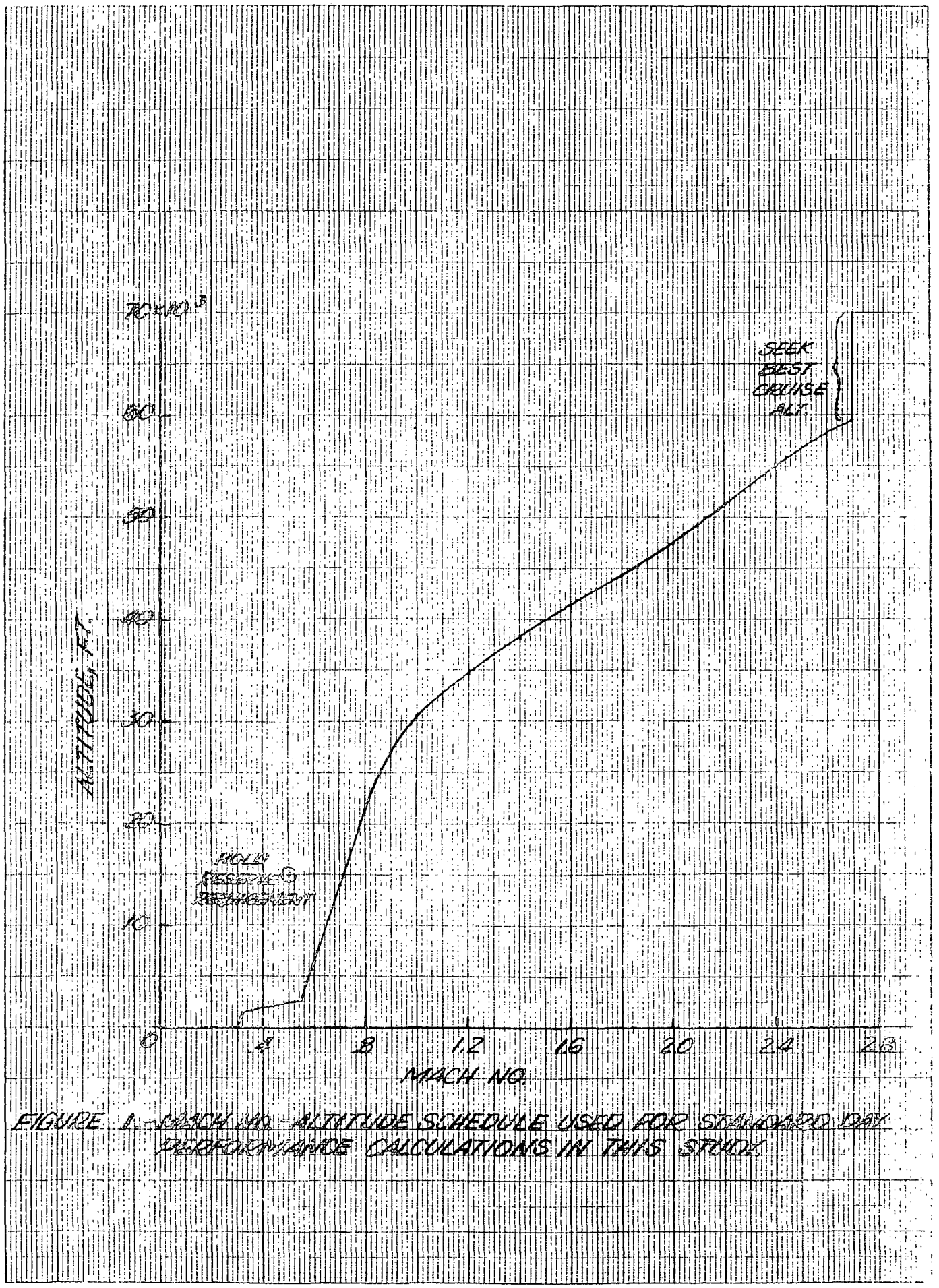

FIGURE 1 MACH NO - ALTITUDE SCHEDULE USED FOR STANDARD DAY PERFORMANCE CALCULATIONS IN THIS STUDY.

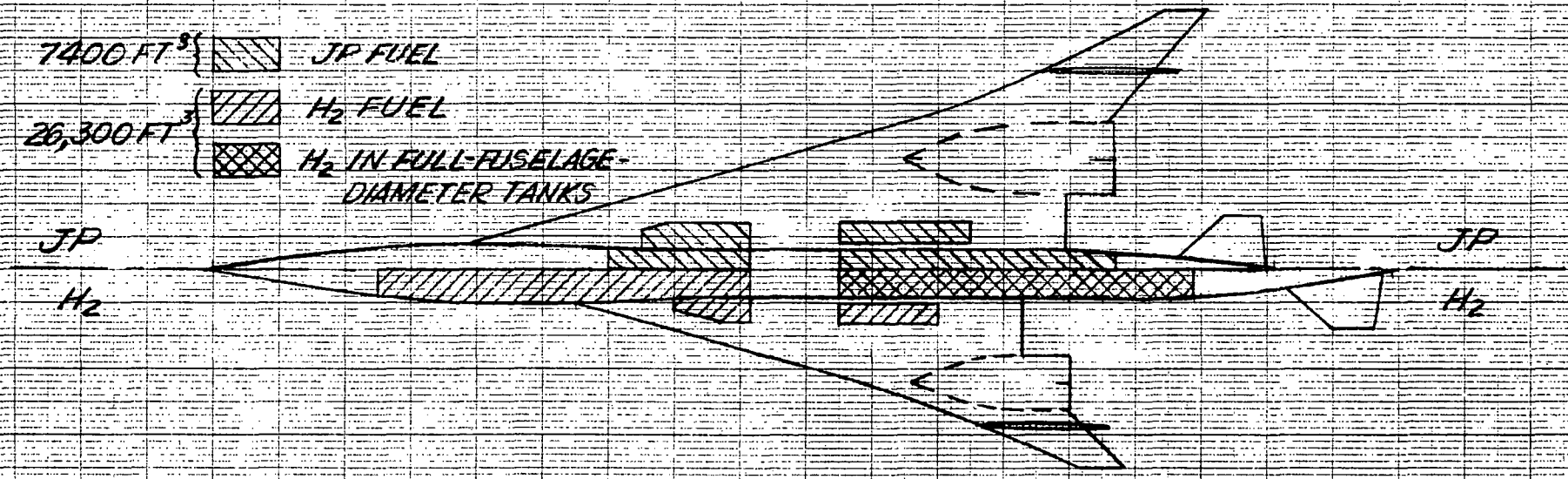

FIGURE 2.— COMPARISON OF JP- AND HYDROGEN-FUELED MACH 2.7 SST'S SHOWING FUEL STORAGE LOCATIONS. DESIGNED FOR 4000-N.MI. RANGE WITH 250 PASSENGERS. TAKEOFF WING LOADING, 60 LB/FT².

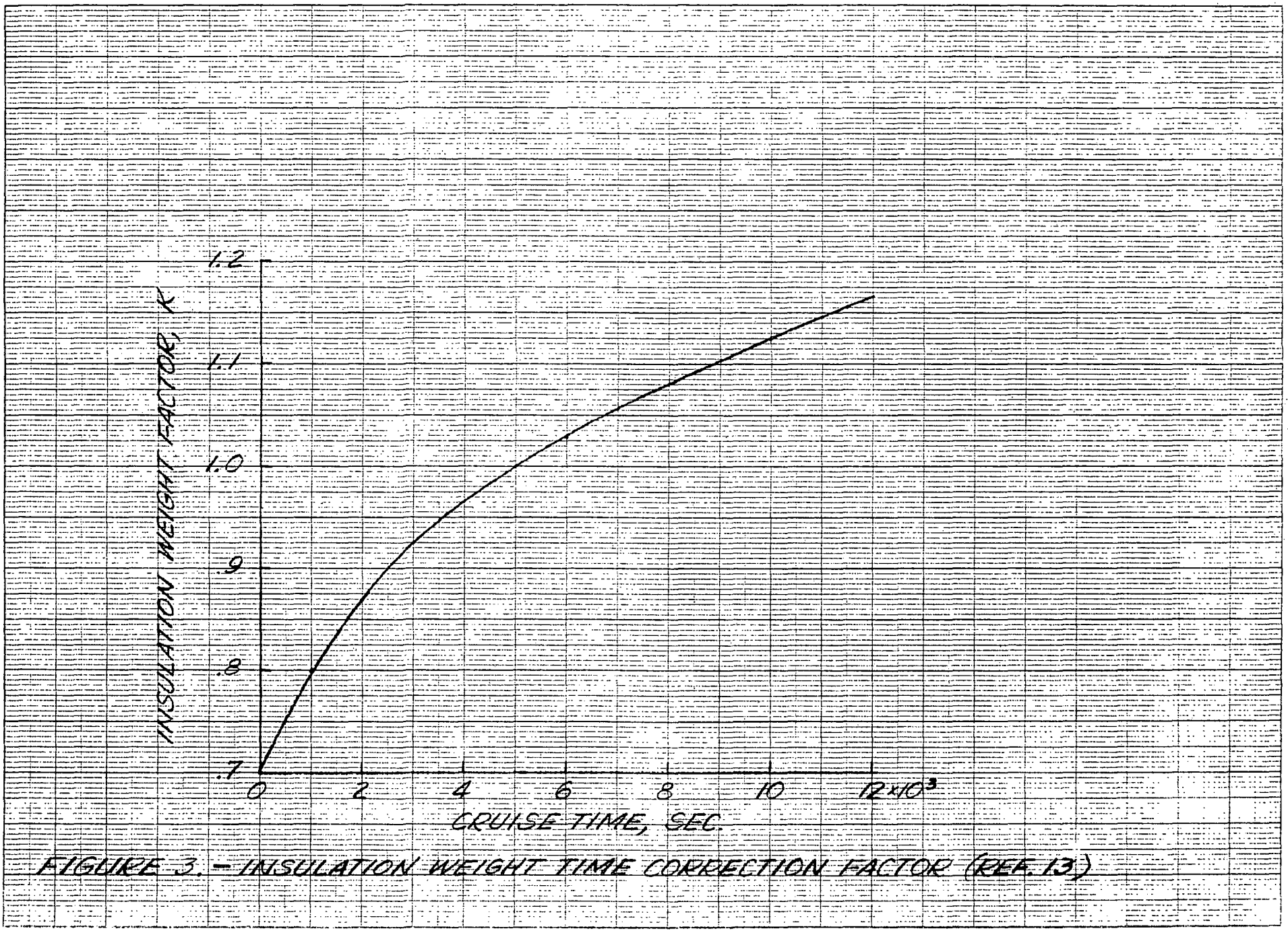

FIGURE 3. - INSULATION WEIGHT TIME CORRECTION FACTOR (REF. 13)

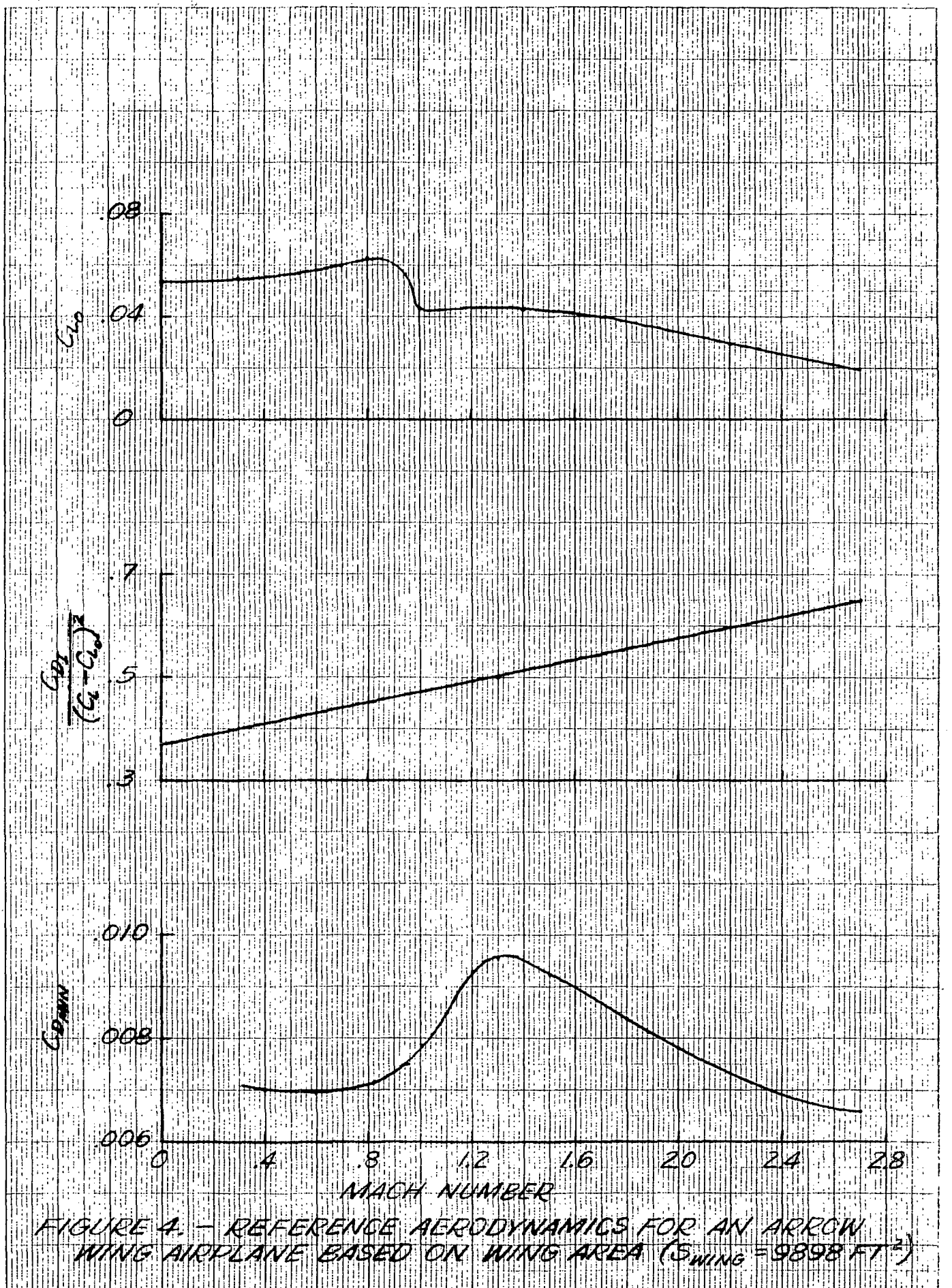

FIGURE 4. – REFERENCE AERODYNAMICS FOR AN ARROW WING AIRPLANE BASED ON WING AREA ($S_{WING} = 9898\ FT^2$)

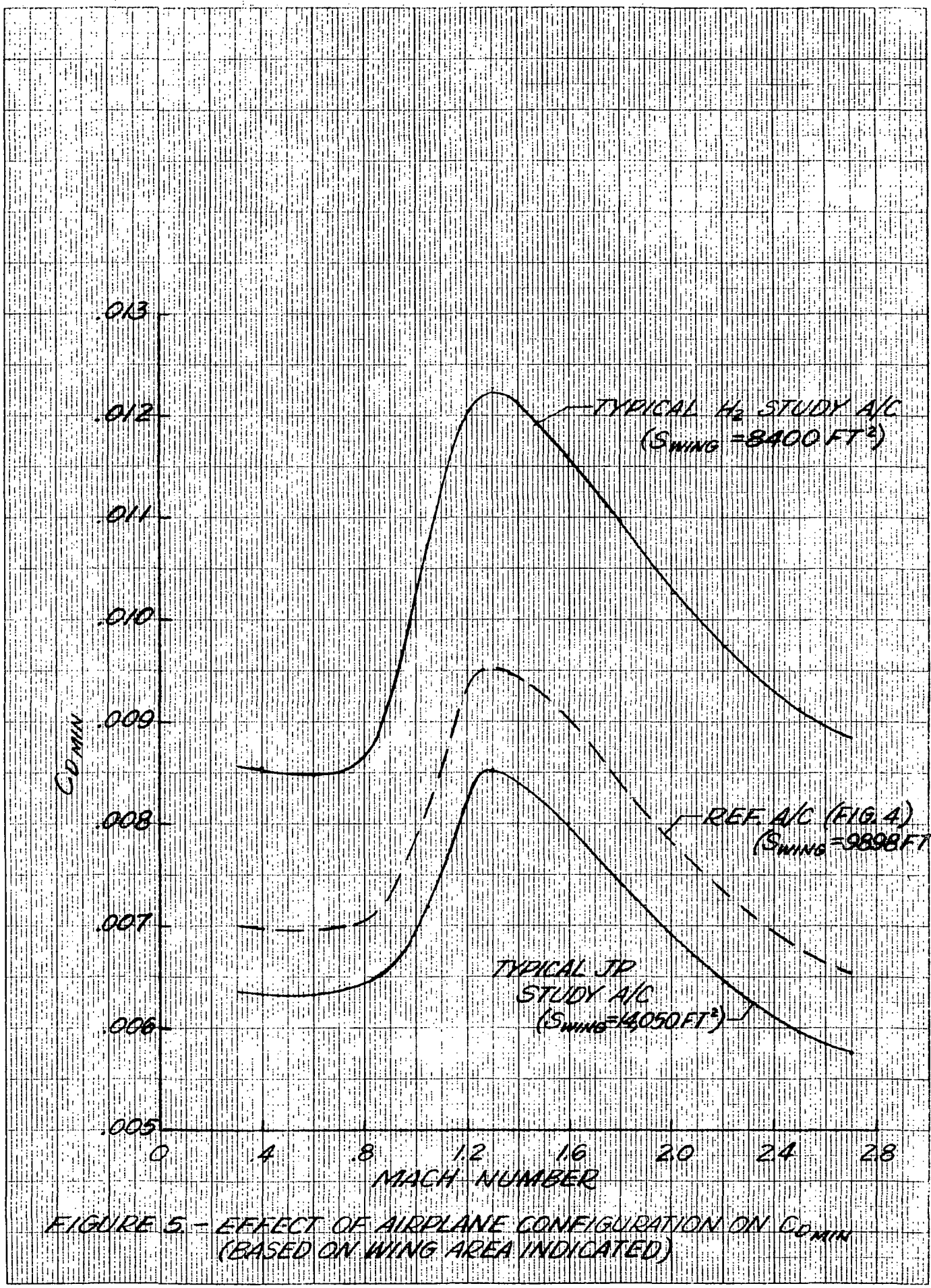

FIGURE 5 - EFFECT OF AIRPLANE CONFIGURATION ON $C_{D_{MIN}}$
(BASED ON WING AREA INDICATED)

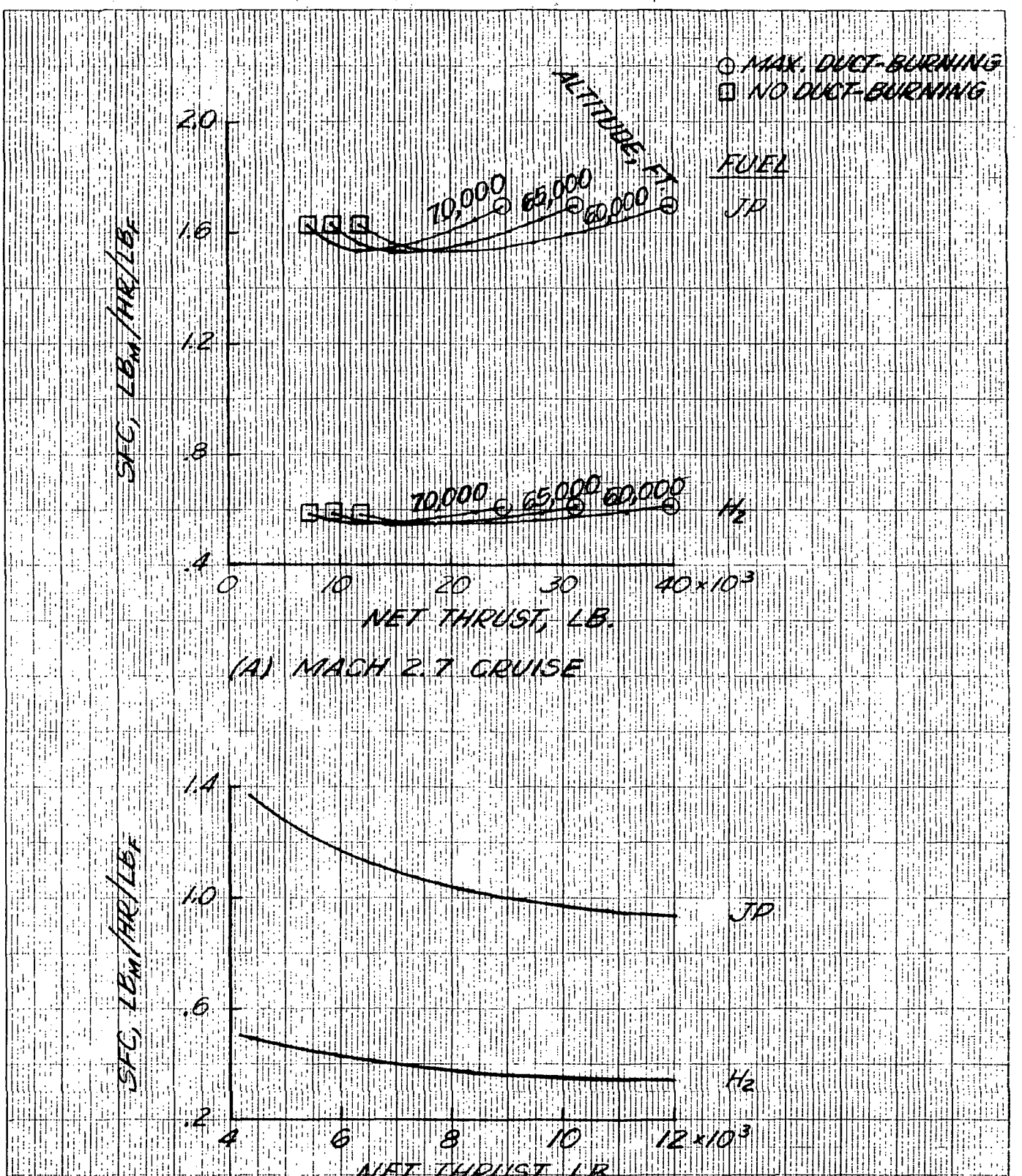

FIGURE 6. - INSTALLED CRUISE PERFORMANCE ON STANDARD DAY. DUCT-BURNING TURBOFAN WITH S.L.S. DESIGN AIRFLOW = 1000 LB/SEC, BYPASS RATIO = 2, FAN PRESSURE RATIO = 3, OVERALL FAN-PLUS-COMPRESSOR PRESSURE RATIO = 10, T_4 = 2725°F.

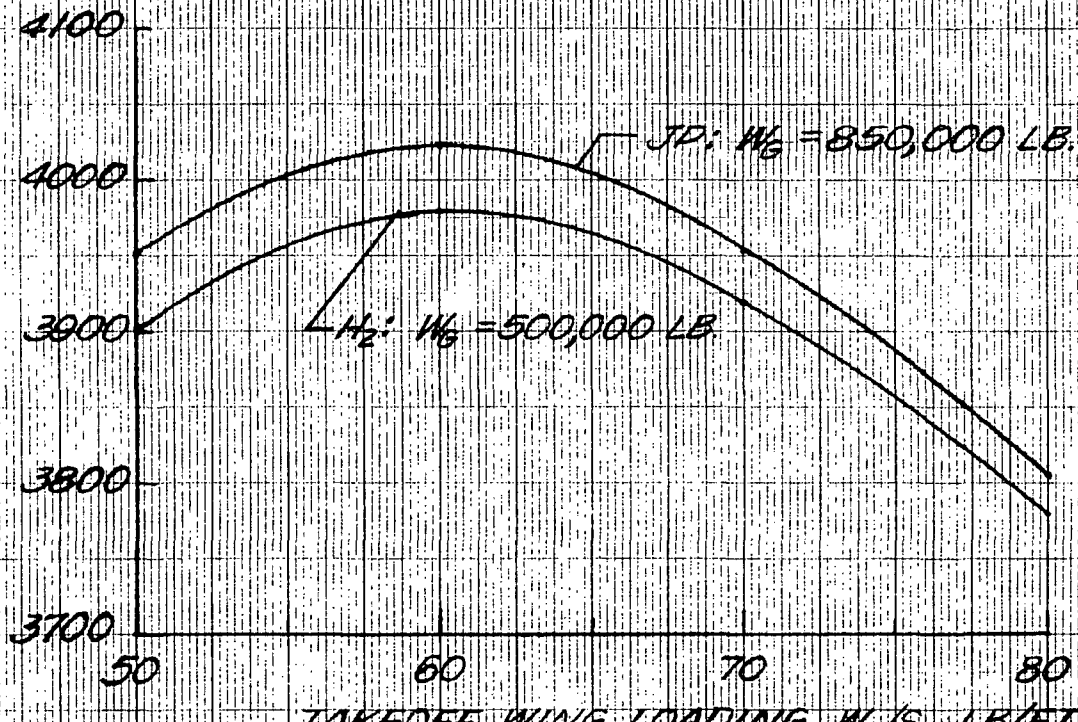

(A) RANGE

FIGURE 7 – OPTIMIZATION OF WING LOADING WITH UNSUPPRESSED DUCT-BURNING TURBOFAN ENGINES. TAKEOFF AT MAXIMUM DRY THRUST. 250 PASSENGERS. DESIGN BPR = 2, FPR = 3, OPR = 10, T_4 = 2725°F.

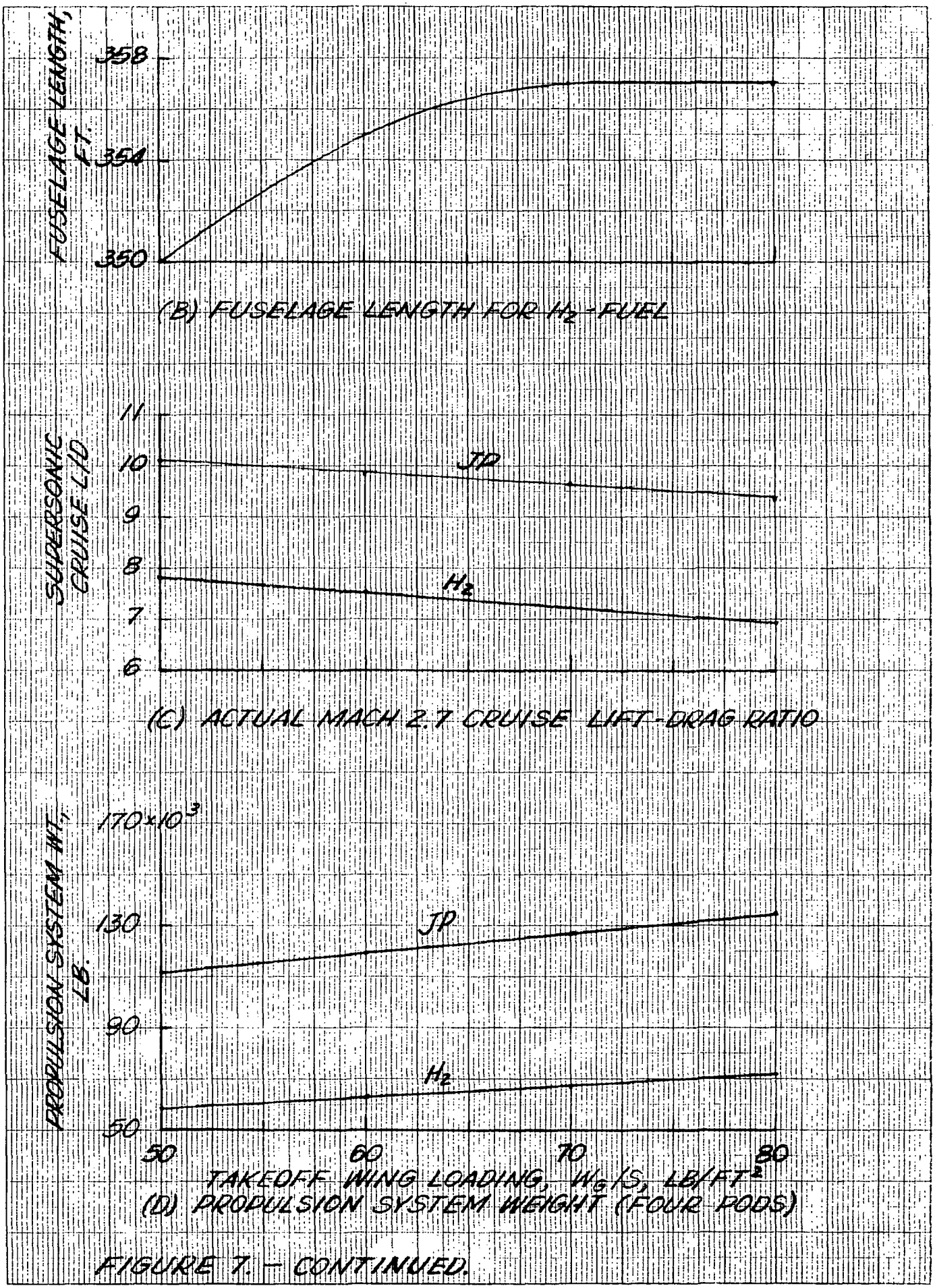

FIGURE 7. — CONTINUED.

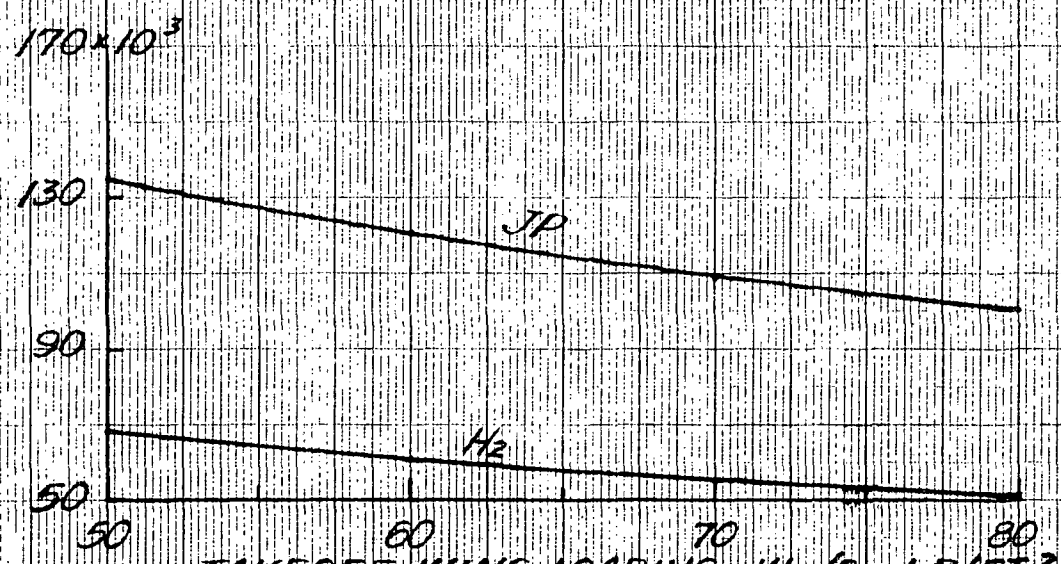

(E) WING WEIGHT

FIGURE 7. – CONCLUDED.

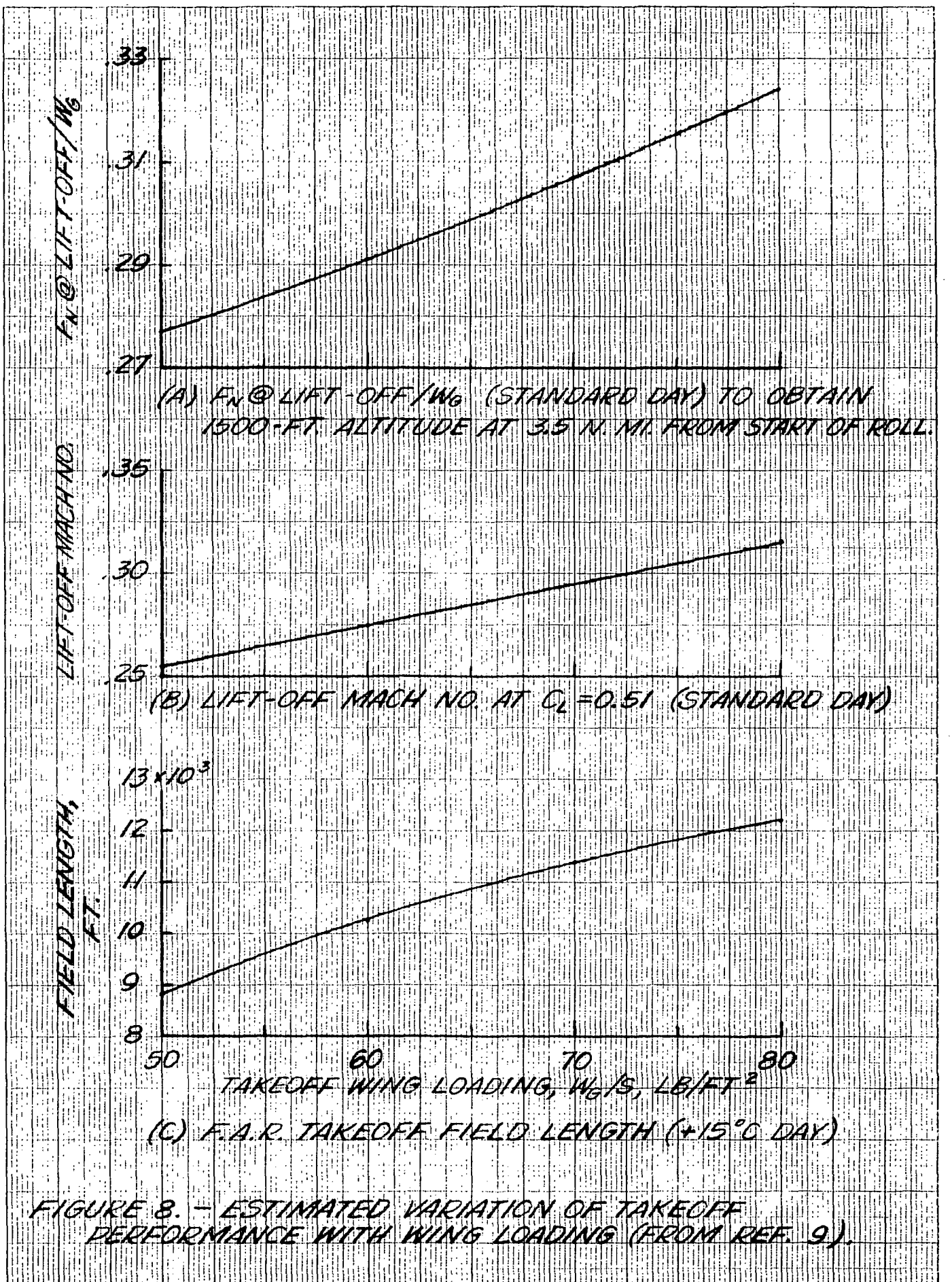

FIGURE 8. – ESTIMATED VARIATION OF TAKEOFF PERFORMANCE WITH WING LOADING (FROM REF. 9).

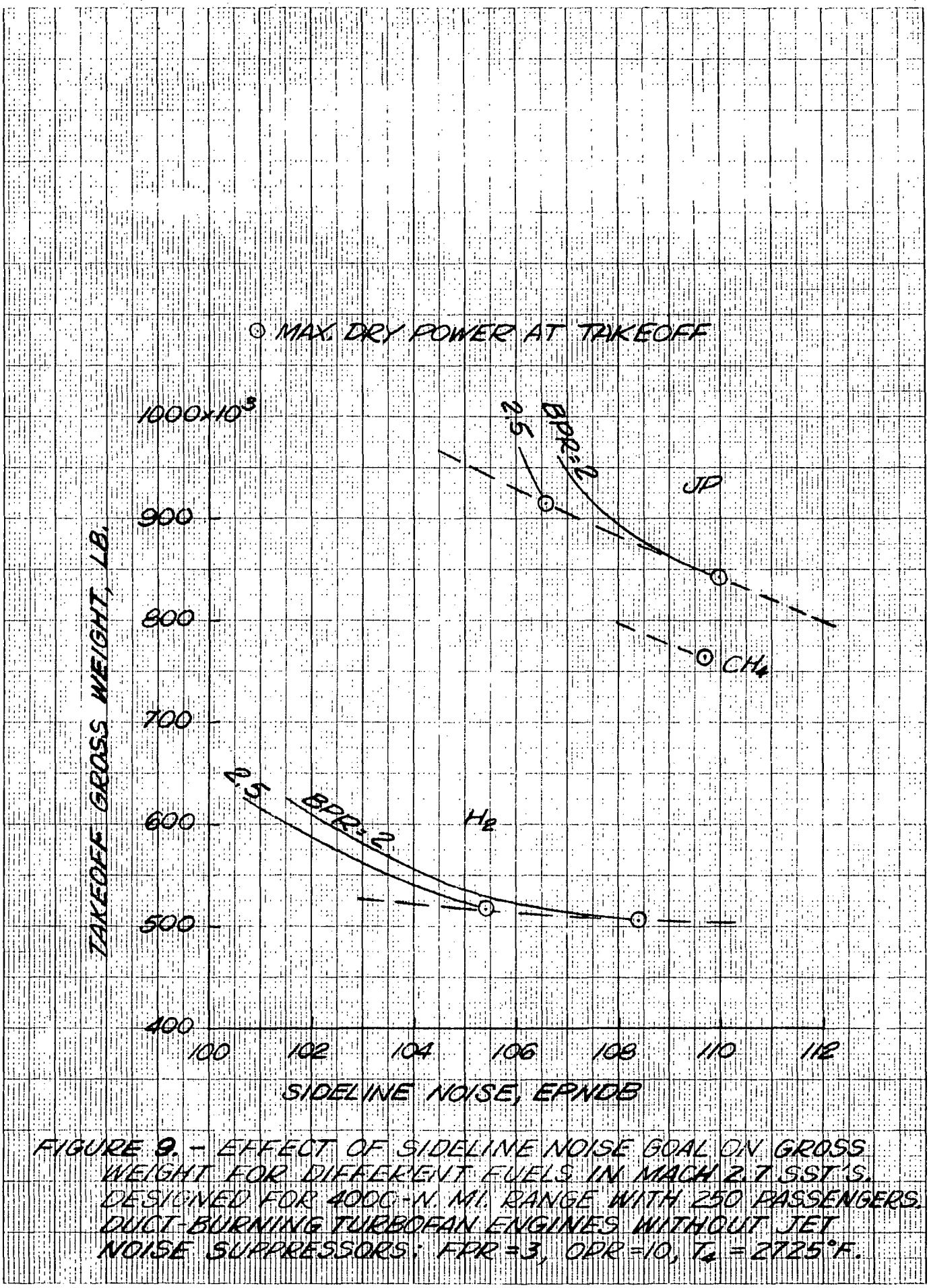

FIGURE 9. – EFFECT OF SIDELINE NOISE GOAL ON GROSS WEIGHT FOR DIFFERENT FUELS IN MACH 2.7 SST'S, DESIGNED FOR 4000-N. MI. RANGE WITH 250 PASSENGERS. DUCT-BURNING TURBOFAN ENGINES WITHOUT JET NOISE SUPPRESSORS: FPR = 3, OPR = 10, T_4 = 2725°F.

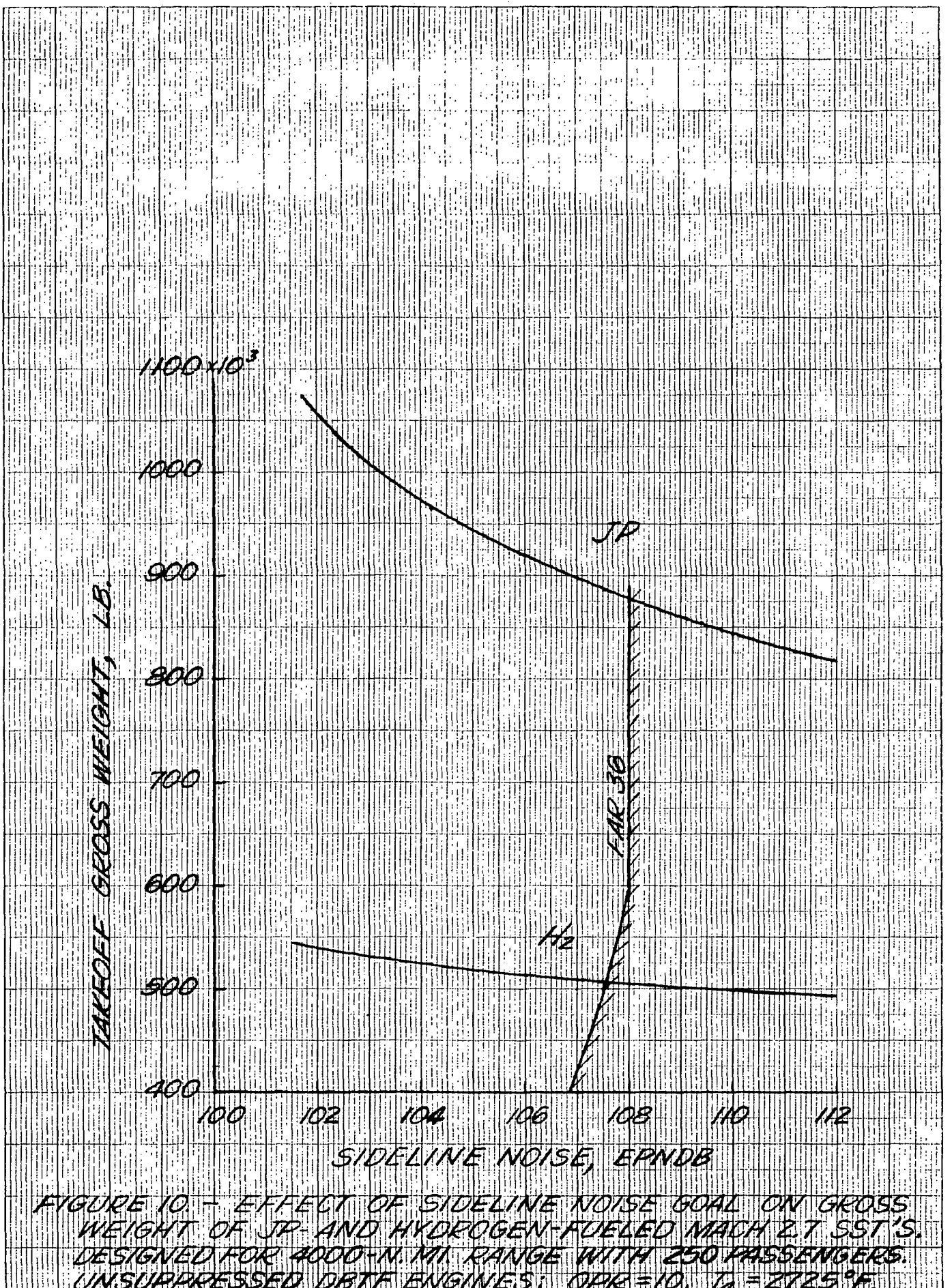

FIGURE 10 – EFFECT OF SIDELINE NOISE GOAL ON GROSS WEIGHT OF JP- AND HYDROGEN-FUELED MACH 2.7 SST'S. DESIGNED FOR 4000-N. MI. RANGE WITH 250 PASSENGERS. UNSUPPRESSED DBTF ENGINES: OPR = 10, T_4 = 2725°F.

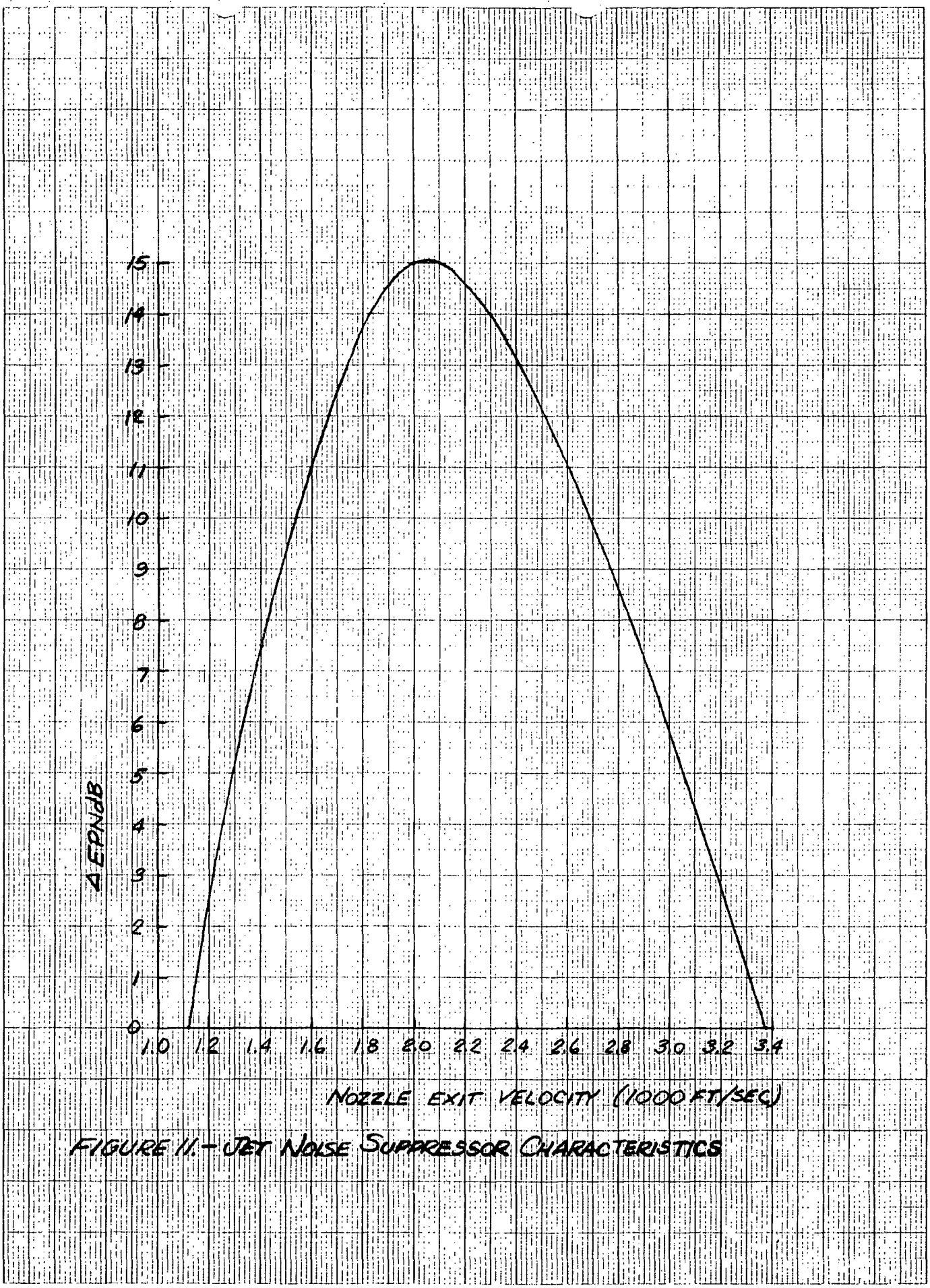

FIGURE 11.- JET NOISE SUPPRESSOR CHARACTERISTICS

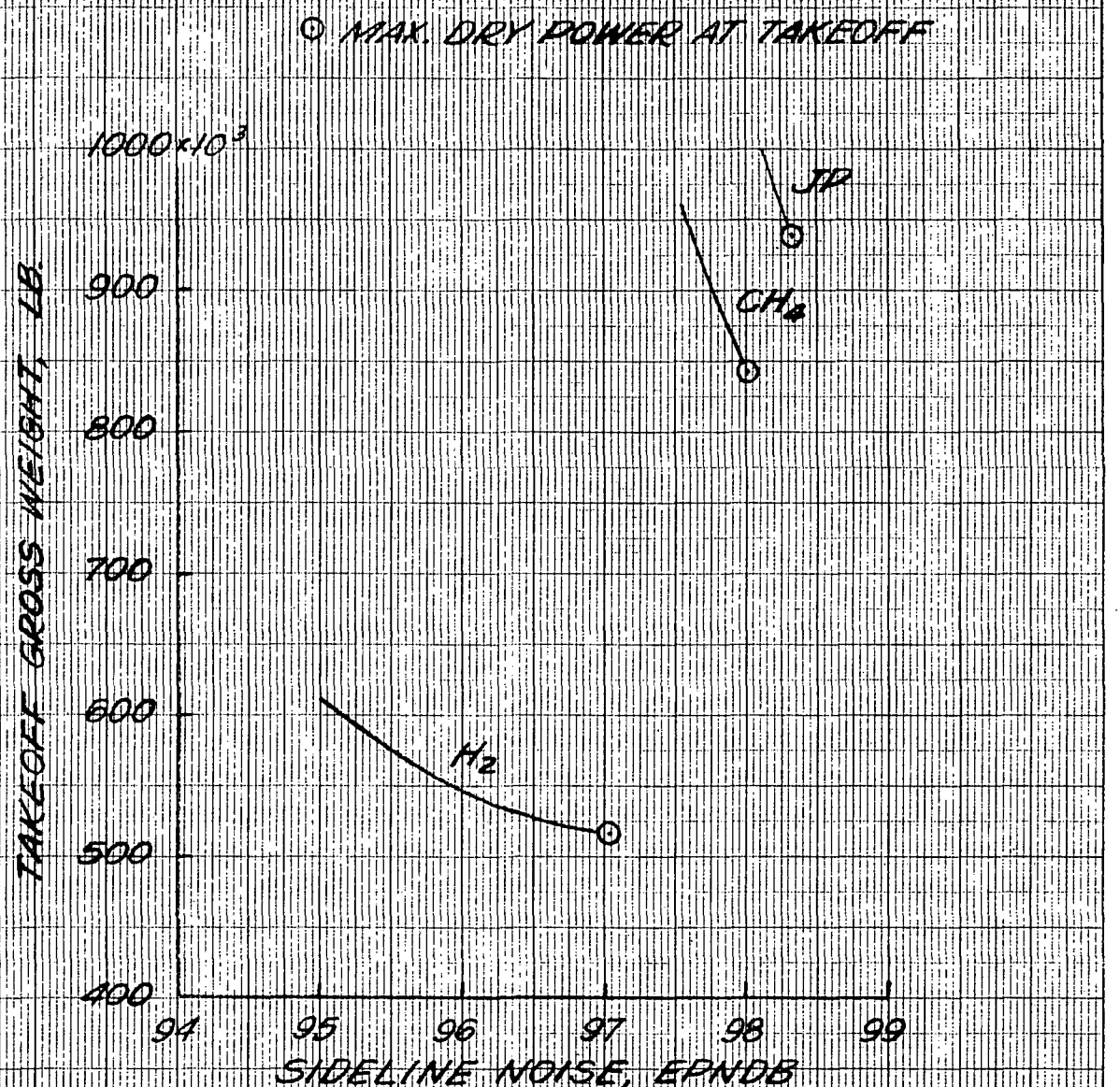

FIGURE 12. — EFFECT OF SIDELINE NOISE GOAL ON GROSS WEIGHT WITH SUPPRESSED ENGINES IN MACH 2.7 SST'S. DESIGNED FOR 4000-N. MI. RANGE WITH 250 PASSENGERS. WEIGHTLESS JET NOISE SUPPRESSORS WITH 7½ PERCENT GROSS THRUST PENALTY. DUCT-BURNING TURBOFAN ENGINES: BPR=2, FPR=3, OPR=10, T_4 = 2725°F.

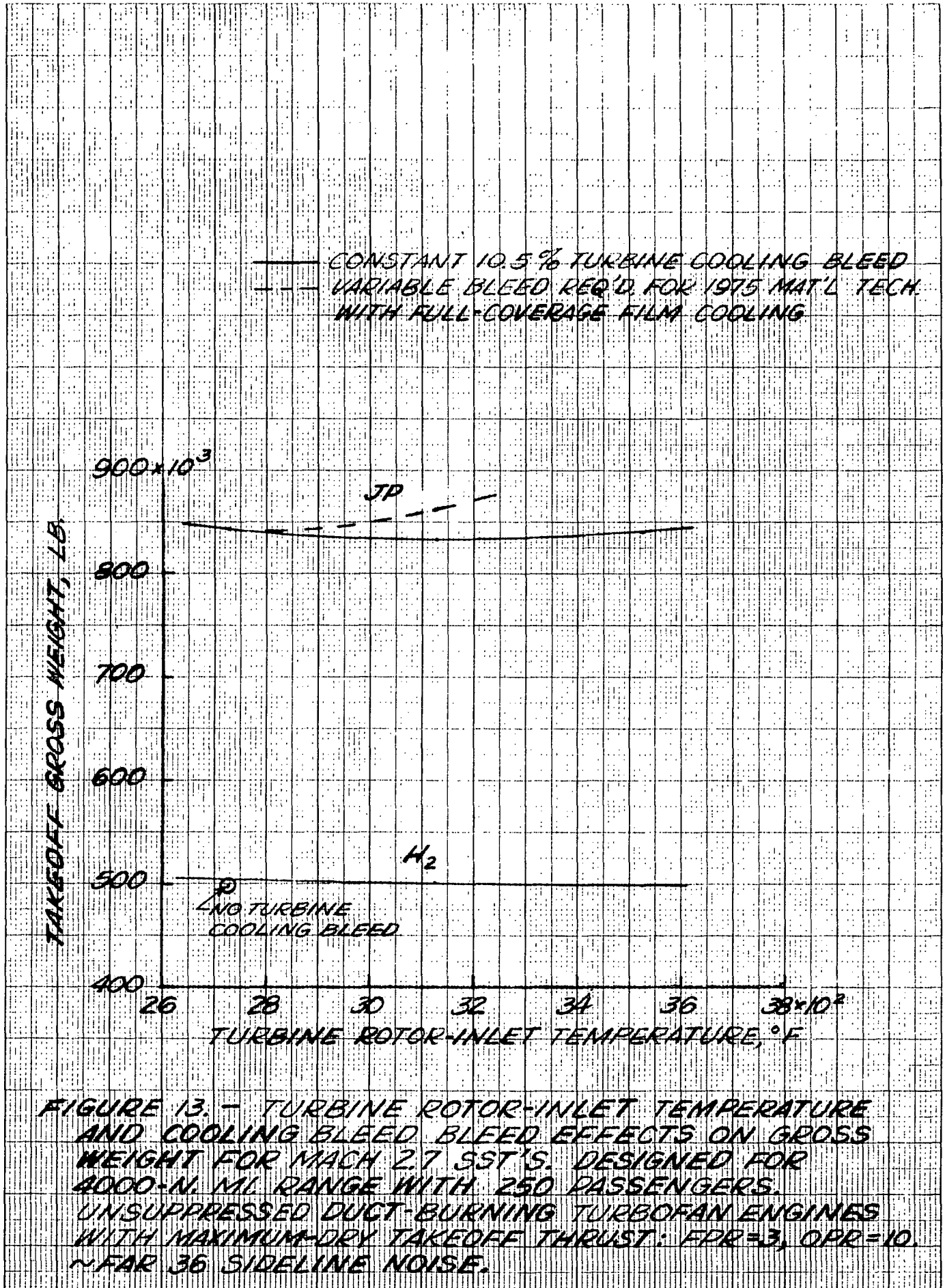

FIGURE 13. – TURBINE ROTOR-INLET TEMPERATURE AND COOLING BLEED BLEED EFFECTS ON GROSS WEIGHT FOR MACH 2.7 SST'S. DESIGNED FOR 4000-N. MI. RANGE WITH 250 PASSENGERS. UNSUPPRESSED DUCT-BURNING TURBOFAN ENGINES WITH MAXIMUM-DRY TAKEOFF THRUST: FPR=3, OPR=10. ~FAR 36 SIDELINE NOISE.

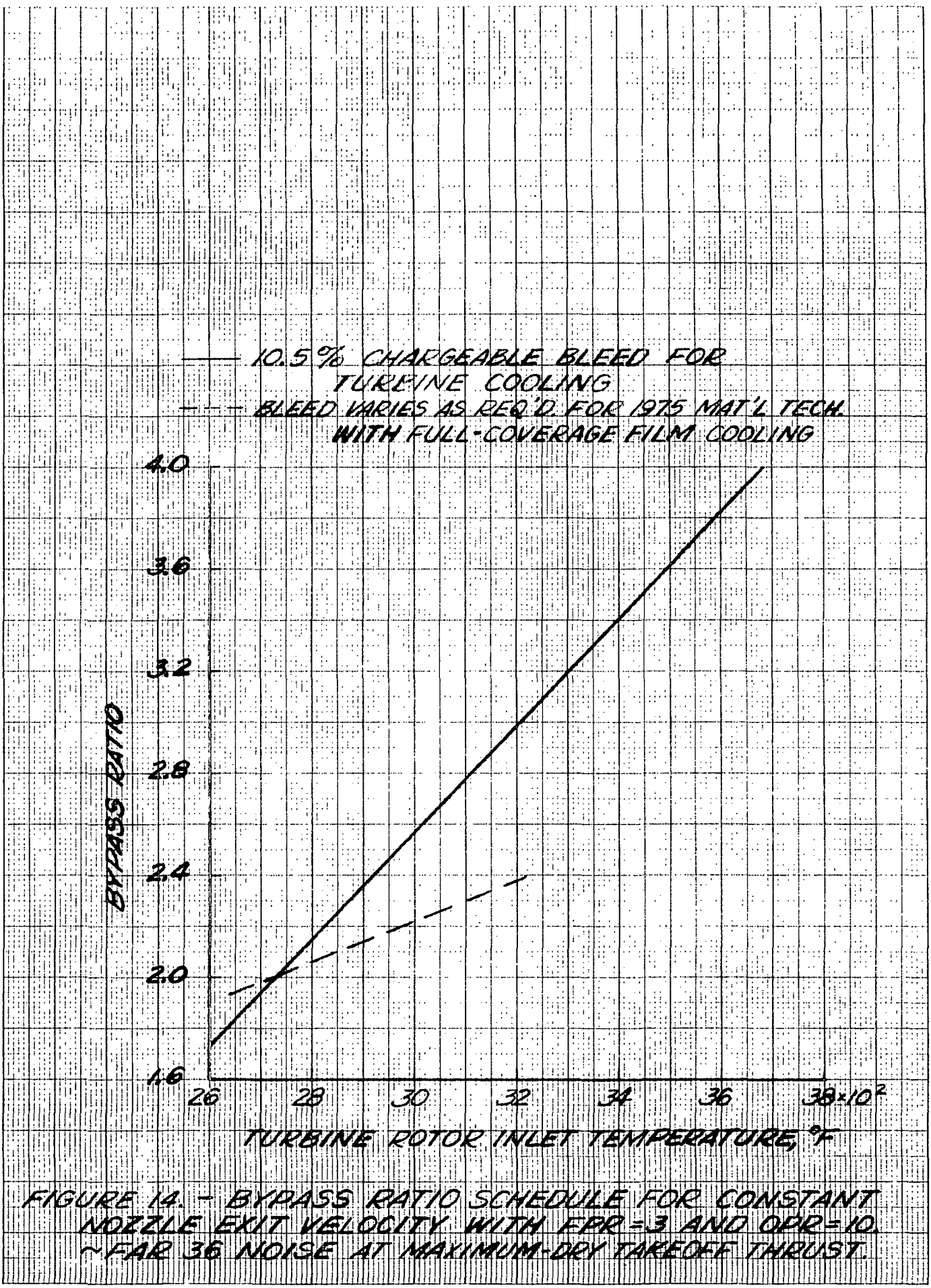

FIGURE 14. – BYPASS RATIO SCHEDULE FOR CONSTANT NOZZLE EXIT VELOCITY WITH FPR=3 AND OPR=10. ~FAR 36 NOISE AT MAXIMUM-DRY TAKEOFF THRUST

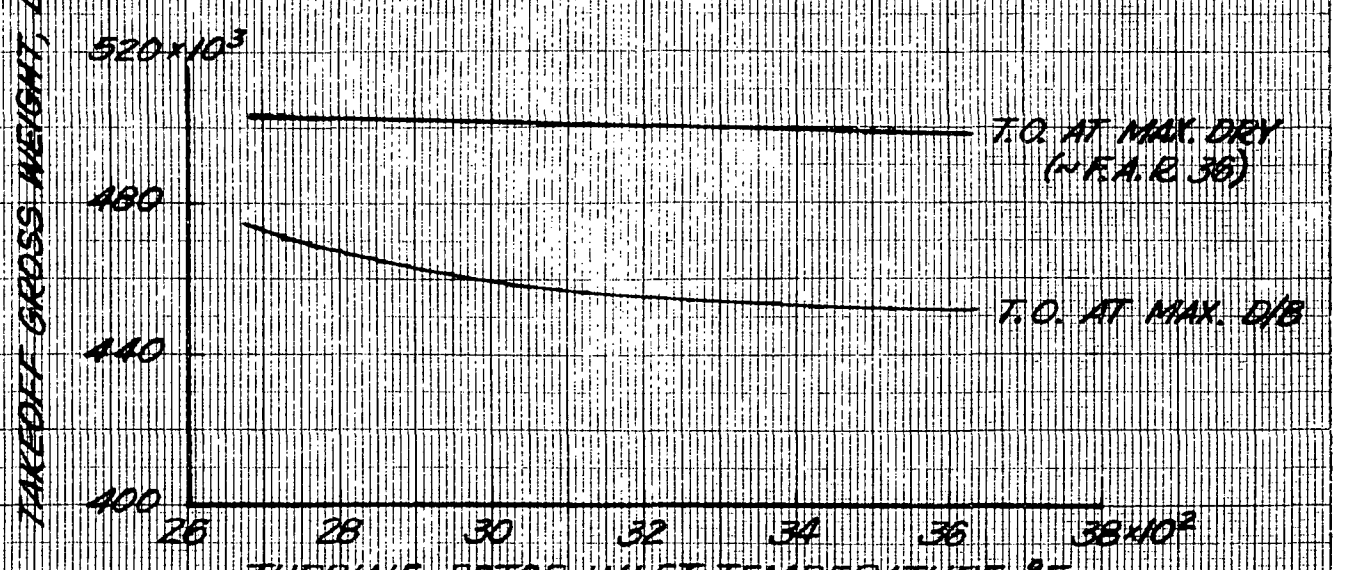

FIGURE 15 – TURBINE ROTOR-INLET-TEMPERATURE EFFECT WHEN TAKEOFF IS UNCONSTRAINED BY FAR 36 SIDELINE NOISE (LOWER CURVE). HYDROGEN-FUELED MACH 2.7 SST'S DESIGNED FOR 4000-N. MI. RANGE WITH 250 PASSENGERS. DUCT-BURNING TURBOFAN ENGINES: FPR = 3, OPR = 10, BPR SCHEDULE FROM FIG. 14 FOR CONSTANT 10.5-PERCENT BLEED. MAXIMUM DUCT-BURNER TEMPERATURE, 2300°F.

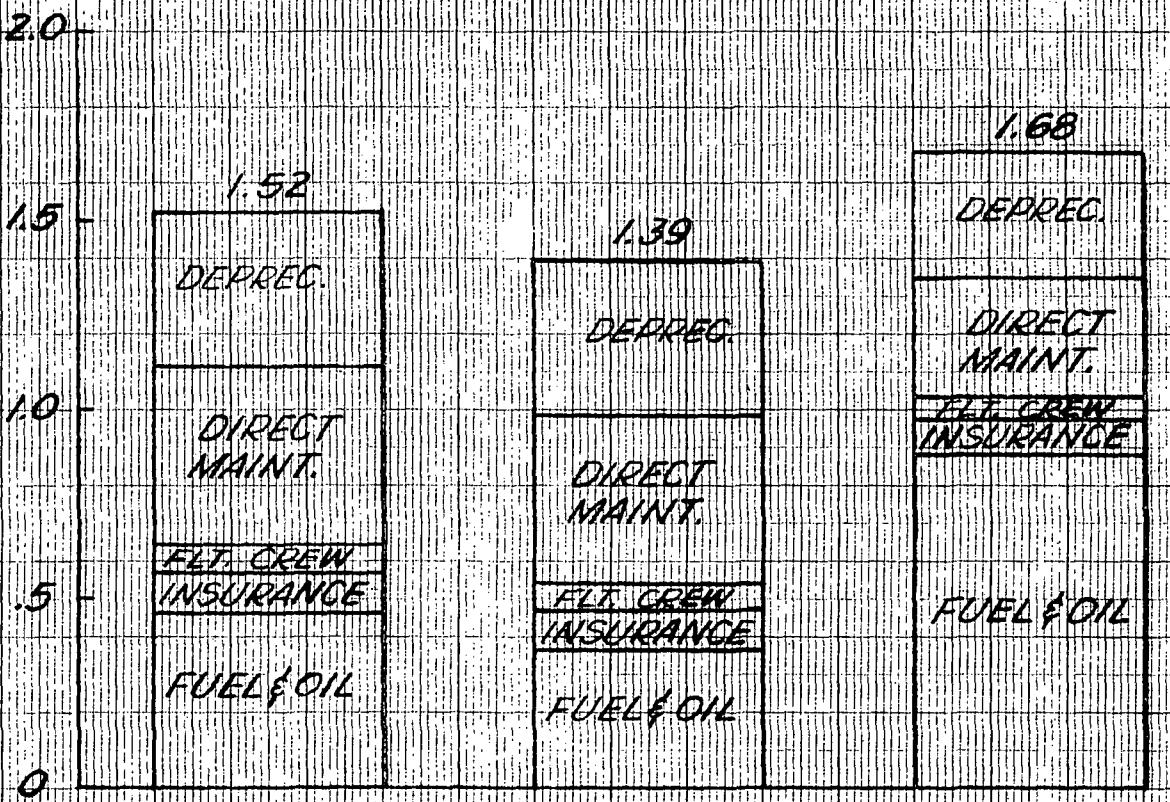

FIGURE 16 – EFFECT OF FUEL TYPE ON DIRECT OPERATING COST OF A MACH-2.7 SST DESIGNED FOR A 4000-N MI. RANGE WITH 250 PASSENGERS. CONSTANT SPECIFIC HARDWARE COST. UNSUPPRESSED DUCT-BURNING TURBOFAN ENGINES: BPR = 2.0, FPR = 3, OPR = 10, T_4 = 2725°F. MAXIMUM DRY TAKEOFF THRUST.

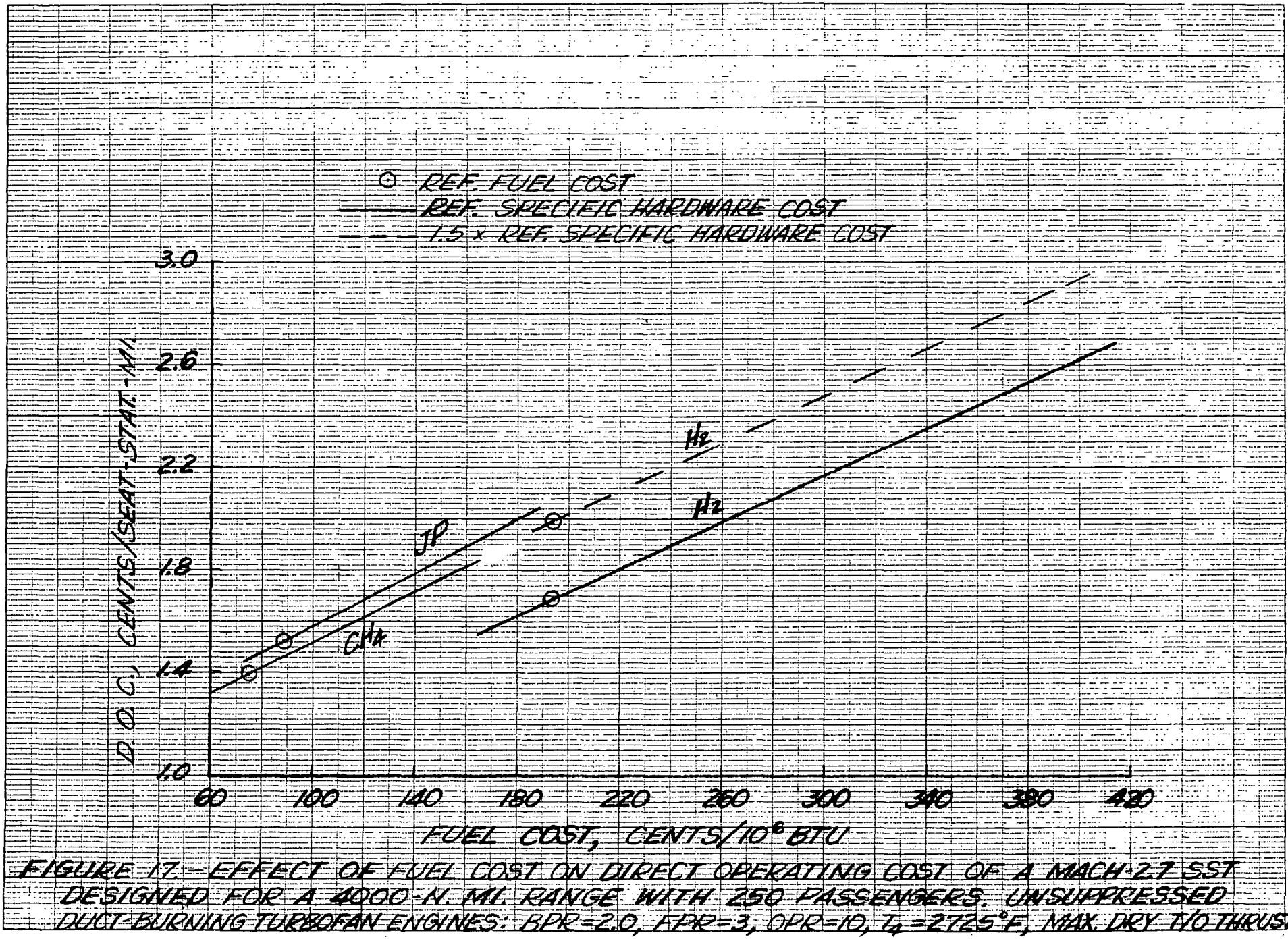

FIGURE 17 – EFFECT OF FUEL COST ON DIRECT OPERATING COST OF A MACH-2.7 SST DESIGNED FOR A 4000-N. MI. RANGE WITH 250 PASSENGERS. UNSUPPRESSED DUCT-BURNING TURBOFAN ENGINES: BPR=2.0, FPR=3, OPR=10, T_4=2725°F, MAX. DRY T/O THRUST.

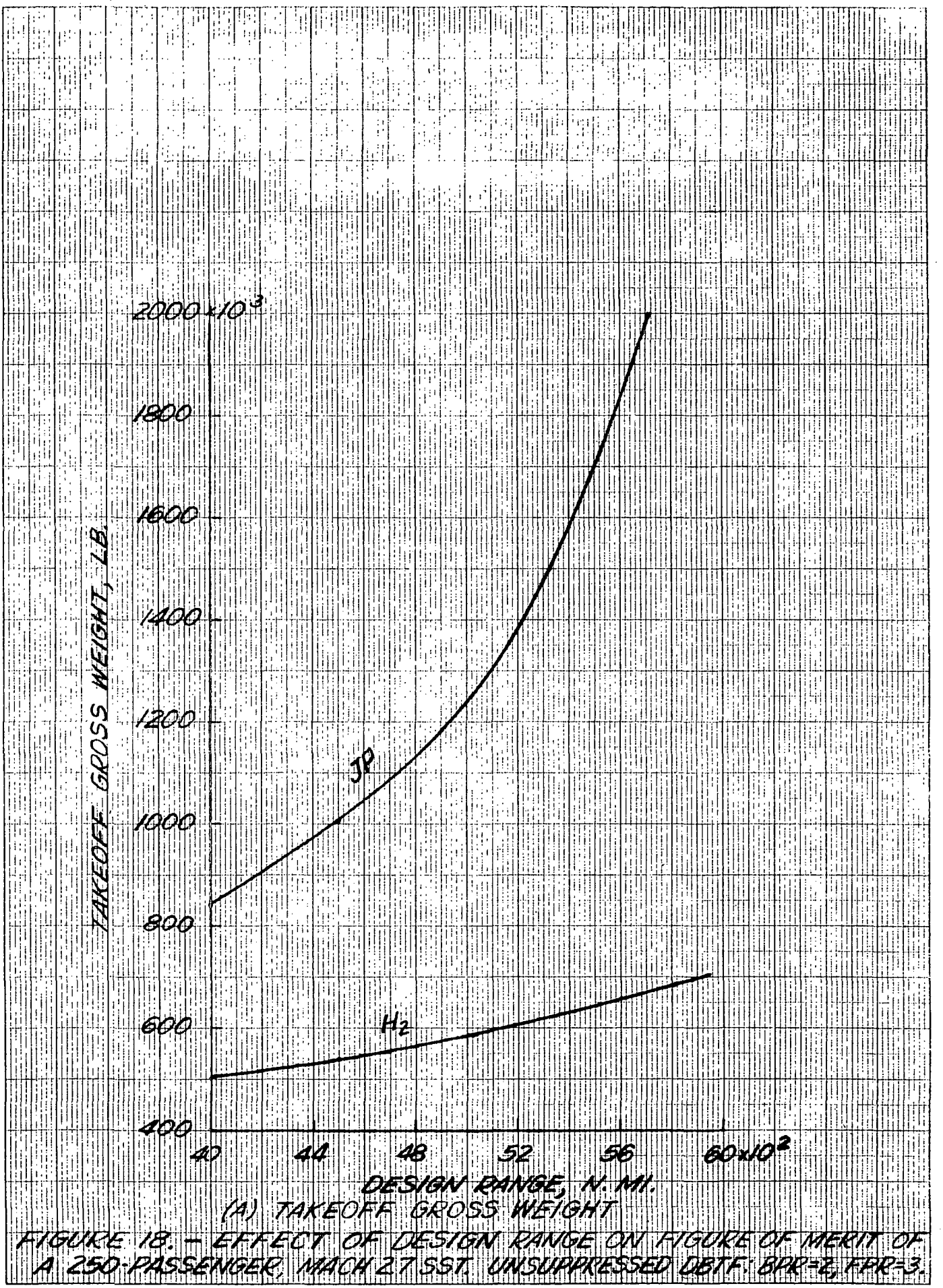

(A) TAKEOFF GROSS WEIGHT

FIGURE 18. - EFFECT OF DESIGN RANGE ON FIGURE OF MERIT OF A 250-PASSENGER MACH 2.7 SST. UNSUPPRESSED DBTF. BPR=2, FPR=3.

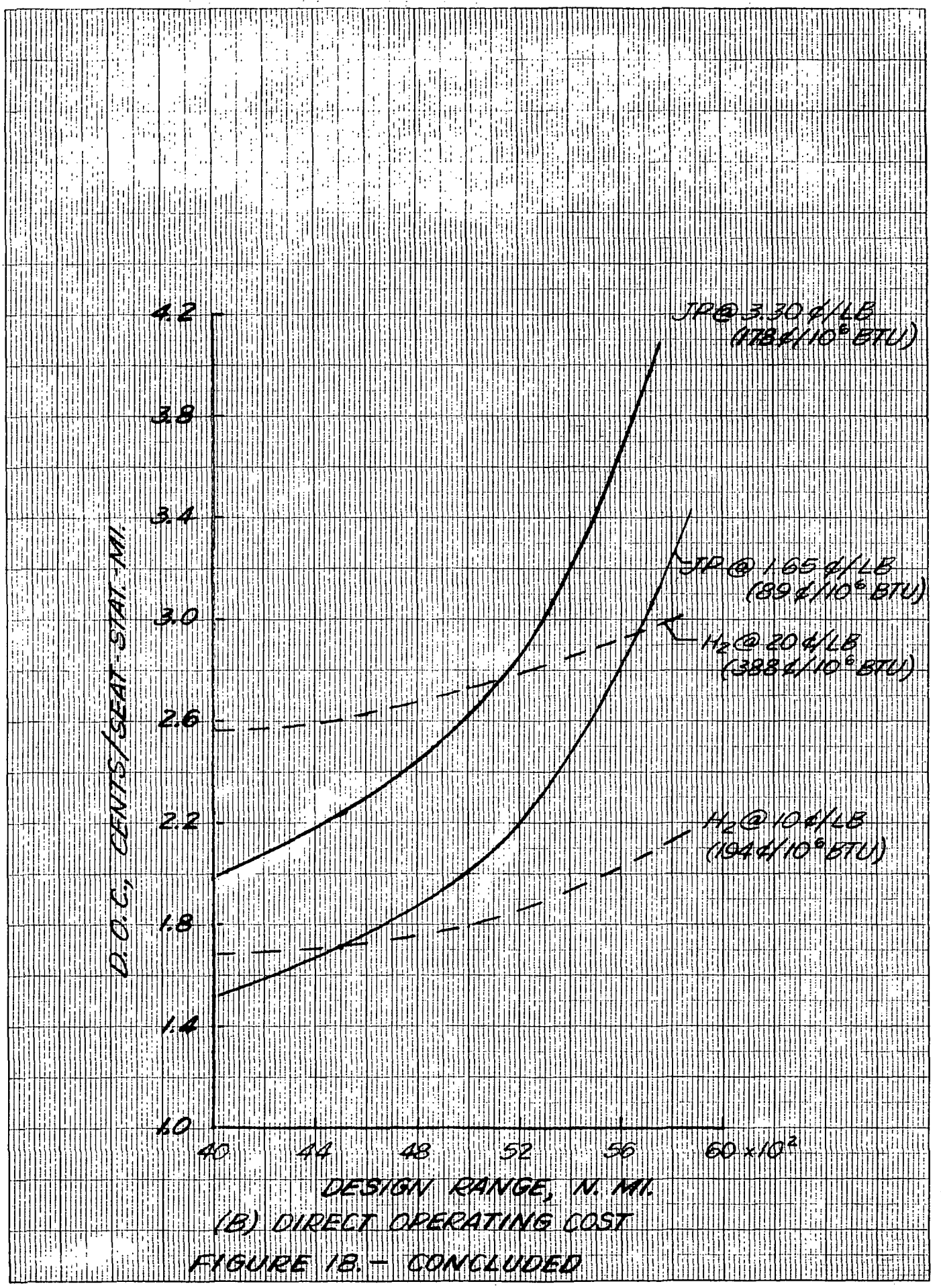

(B) DIRECT OPERATING COST

FIGURE 18.- CONCLUDED

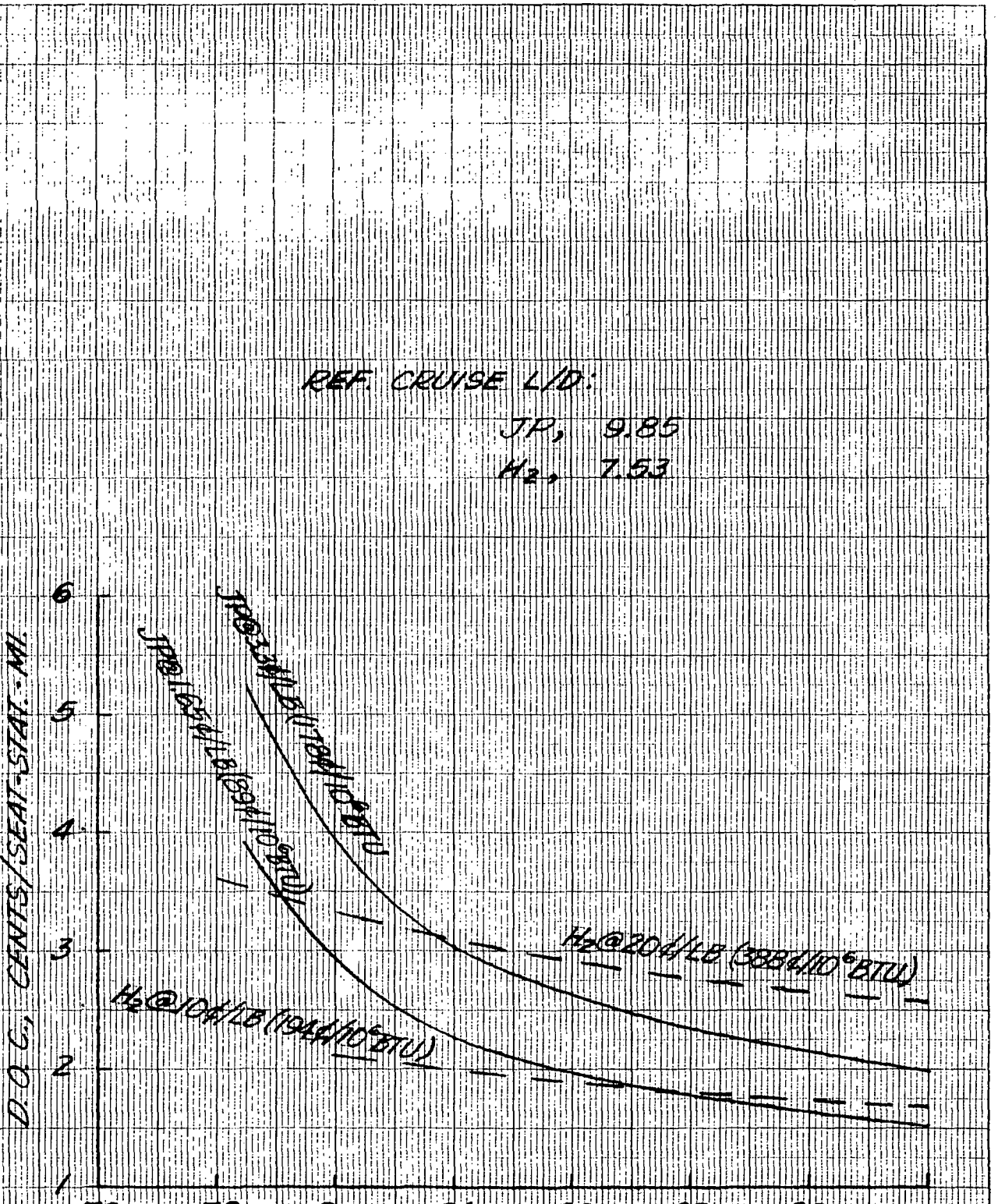

FIGURE 19. – EFFECT OF CRUISE LIFT-DRAG RATIO ASSUMPTIONS ON DIRECT OPERATING COST OF A 250-PASSENGER, MACH-2.7 SST. UNSUPPRESSED DUCT-BURNING TURBOFAN ENGINES: BPR = 2.0, FPR = 3, OPR = 10, T_4 = 2725°F. MAXIMUM DRY TAKEOFF THRUST.